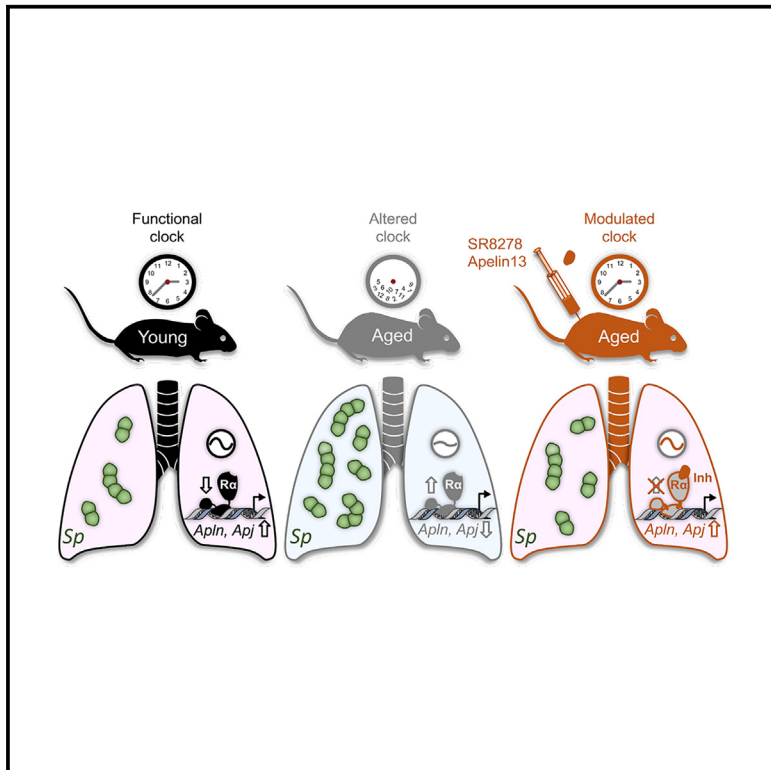


Rev-erb- α antagonism in alveolar macrophages protects against pneumococcal infection in elderly mice

Graphical abstract



Authors

Fabiola Silva Angulo,
Claudine Vanessa Joseph, Lou Delval, ...,
Hélène Duez, Benoit Pourcet,
François Trottein

Correspondence

helene.duez@inserm.fr (H.D.),
benoit.pourcet@univ-lille.fr (B.P.),
francois.trottein@pasteur-lille.fr (F.T.)

In brief

Silva Angulo et al. provide insights into mechanisms underlying respiratory bacterial susceptibility in the elderly. The authors demonstrate that the altered circadian expression of the nuclear receptor Rev-erb- α and the apelin/apelin receptor (APJ) in aged lungs associates with dysregulated time-of-day control of pulmonary immune defenses against pneumococcal infections.

Highlights

- Rev-erb- α and apelin/APJ are among the most dysregulated circadian genes in aged lungs
- Rev-erb- α antagonism protects against infection by activating alveolar macrophages
- The Rev-erb- α /APJ pathway plays a role in pulmonary defense against pneumococcal infection
- The Rev-erb- α antagonist SR8278 protects against pneumococcal infection in elderly mice



Article

Rev-erb- α antagonism in alveolar macrophages protects against pneumococcal infection in elderly mice

Fabiola Silva Angulo,¹ Claudine Vanessa Joseph,¹ Lou Delval,¹ Lucie Deruyter,¹ Séverine Heumel,¹ Marie Bicharel,² Patricia Brito Rodrigues,¹ Valentin Sencio,¹ Tom Bourguignon,³ Marina Gomes Machado,¹ Marie Fourcot,⁴ Stéphane Delhay,² Sophie Salomé-Desnoulez,⁴ Philippe Valet,⁵ Serge Adnot,⁶ Isabelle Wolowczuk,¹ Jean-Claude Sirard,¹ Muriel Pichavant,¹ Bart Staels,² Joel T. Haas,² Ruxandra Gref,³ Jimmy Vandel,⁴ Arnaud Machelart,¹ Hélène Duez,^{2,*} Benoit Pourchet,^{2,7,*} and François Trottein^{1,7,8,*}

¹University Lille, CNRS, INSERM, CHU Lille, Institut Pasteur de Lille, U1019 - UMR 9017 - CIIL - Center for Infection and Immunity of Lille, 59000 Lille, France

²University Lille, INSERM, CHU Lille, Institut Pasteur de Lille, U1011 - EGID, 59000 Lille, France

³University Paris Saclay, CNRS, UMR 8214 - Institute of Molecular Sciences, 91400 Orsay, France

⁴University Lille, CNRS, INSERM, CHU Lille, Institut Pasteur de Lille, US 41 - UAR 2014 - PLBS, 59000 Lille, France

⁵University Paul Sabatier, University Toulouse, INSERM, CNRS, U1301 - UMR 5070 - Institut RESTORE, 31000 Toulouse, France

⁶University Paris-Est Créteil, INSERM, U955, Institut Mondor de Recherche Biomédicale, 94010 Créteil, France

⁷These authors contributed equally

⁸Lead contact

*Correspondence: helene.duez@inserm.fr (H.D.), benoit.pourchet@univ-lille.fr (B.P.), francois.trottein@pasteur-lille.fr (F.T.)

<https://doi.org/10.1016/j.celrep.2025.115273>

SUMMARY

Circadian rhythms control the diurnal nature of many physiological, metabolic, and immune processes. We hypothesized that age-related impairments in circadian rhythms are associated with high susceptibility to bacterial respiratory tract infections. Our data show that the time-of-day difference in the control of *Streptococcus pneumoniae* infection is altered in elderly mice. A lung circadian transcriptome analysis revealed that aging alters the daily oscillations in the expression of a specific set of genes and that some pathways that are rhythmic in young-adult mice are non-rhythmic or time shifted in elderly mice. In particular, the circadian expression of the clock component Rev-erb- α and apelin/apelin receptor was altered in elderly mice. In young-adult mice, we discovered an interaction between Rev-erb- α and the apelinergic axis that controls host defenses against *S. pneumoniae* via alveolar macrophages. Pharmacological repression of Rev-erb- α in elderly mice resulted in greater resistance to pneumococcal infection. These data suggest the causative role of age-associated impairments in circadian rhythms on respiratory infections and have clinical relevance.

INTRODUCTION

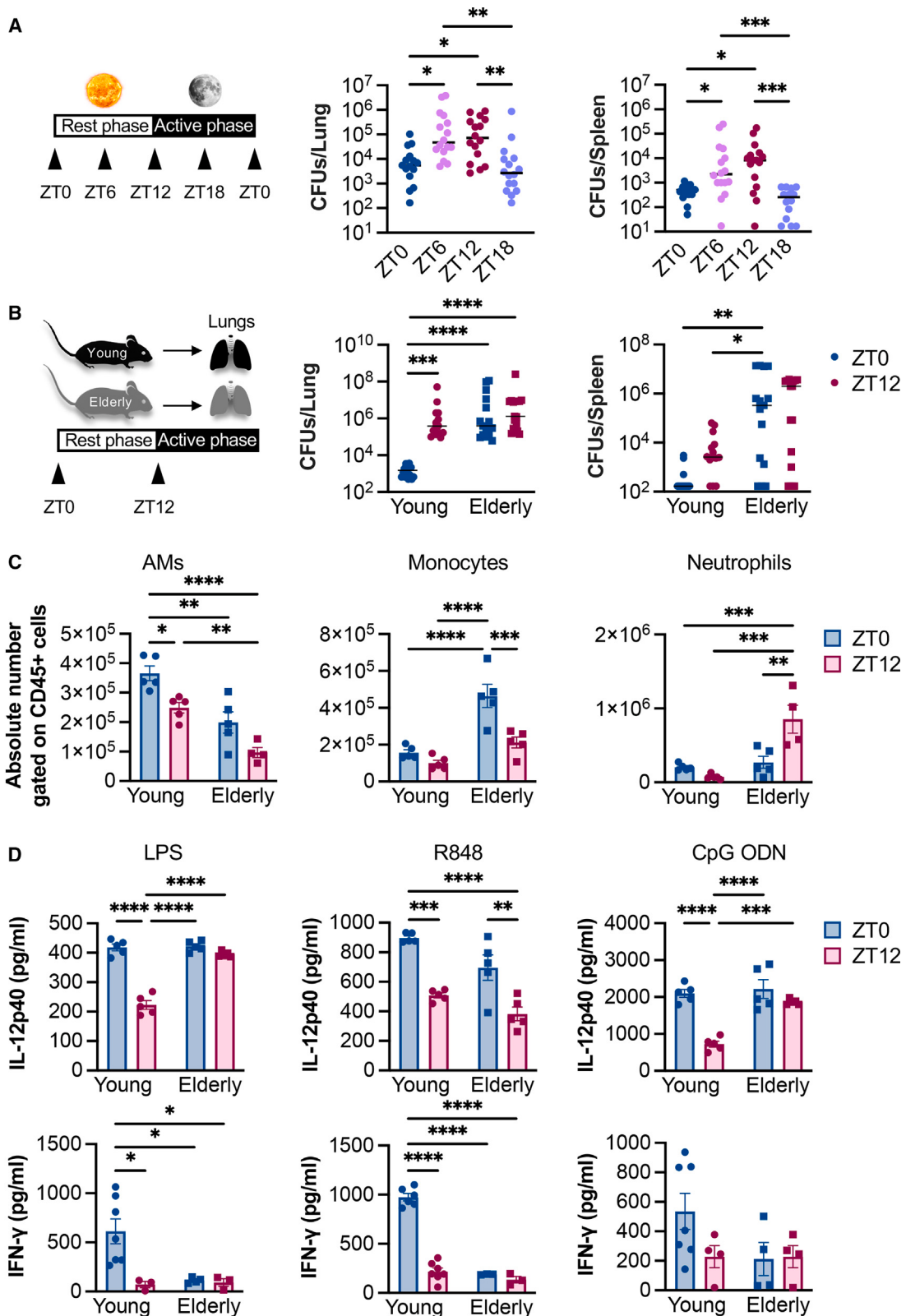
Immune-function dysregulation has a major impact on age-related diseases, with an elevation in the risk of cancer and cardiovascular, metabolic, and neurodegenerative pathologies. Furthermore, age-mediated alterations in immune function increase susceptibility to infections in general and lung infections in particular. Indeed, older adults are more vulnerable than the general population to respiratory pathogens such as *Streptococcus pneumoniae*, the most common cause of community-acquired bacterial pneumonia.¹ As life expectancy increases and the number of older adults grows, a better understanding of the causes and mechanisms involved in this age-related elevation in susceptibility to bacterial pathogens is critical for the development of new treatments. While the reasons of the increased susceptibility to infection in the elderly are likely multifactorial, the underlying mechanisms are mainly related to impaired pulmonary

functions (poor mucociliary clearance and a weak barrier) and impairments in innate and adaptive immunity in the aging lung.^{2–5}

The objective of the present study was to determine whether age-related changes in circadian rhythms contribute to susceptibility to respiratory infections in elderly mice.

Circadian rhythms are daily oscillations in several biological processes. These oscillations allow organisms to anticipate and adapt to environmental changes that occur during a 24-h period.^{6,7} Circadian rhythms are generated by an endogenous biological clock that has been well conserved over the course of evolution. The central pacemaker that receives light information and synchronizes clocks throughout the body is located in the suprachiasmatic nuclei of the hypothalamus. In addition, all mammalian cells (including immune cells) harbor a functional circadian clock, which generates circadian oscillations in the transcriptome, proteome, and, thus, cell/tissue functions.⁸ On the molecular level, the circadian clock consists of a complex





(legend on next page)

network of transcription factors organized in interconnected positive and negative feedback loops and that generate rhythms with a 24-h period.⁹ The positive feedback limb is driven by the heterodimer complex brain and muscle ARNT-like 1 (Bmal1) and circadian locomotor output cycle kaput (Clock), which binds to E boxes in the promoter of its target genes. The latter include the Period1/2/3 (Per) and Cryptochrome1/2 (Cry) clock genes, which form the negative feedback limb. Once they reach a sufficient threshold, the Per and Cry proteins heterodimerize and the complex translocates into the nucleus, quenches the Bmal1/Clock heterodimer, and thus inhibits its transcriptional activity. Other transcription factors including nuclear receptor families Rev-erb and retinoic acid receptor-related orphan receptors (RORs) are strong modulators of the molecular clock and can fine-tune the circadian circuitry.¹⁰ These nuclear receptors control the expression of many genes and thereby generate rhythmic oscillations in transcriptional programs and specific tissue functions, including those in the lungs.^{11,12} It is estimated that the expression of approximately 80% of genes oscillates in a daily manner at one body site at least.¹³ Rev-erb- α is not only important in generating circadian rhythmicity by inhibiting the expression of Bmal1 and Clock but is also critical in metabolic and inflammation/repair processes.^{14–20} We have shown that Rev-erb- α in mice is critical in acute and chronic inflammatory diseases, including fulminant hepatitis²¹ and atherosclerosis.²²

The biological clock controls host defenses against pathogens,^{14,23–25} including *S. pneumoniae*.^{11,26,27} It regulates many immune functions over the circadian cycle, including immune cell infiltration, pattern recognition receptor expression, cytokine secretion, and phagocytosis.^{8,28–32} A robust circadian system is therefore essential for good health and longevity.³³ However, circadian rhythms are impaired by several conditions, including shift work, erratic light exposure, changes in feeding behavior, consumption of a high-fat diet, social jetlag, and aging.^{34,35} Clock disruption has been implicated in the pathogenesis of chronic metabolic and inflammatory diseases.^{34,35} In older adults, disruption of normal circadian rhythms is associated with clinically relevant disorders, including neurodegeneration and metabolic/inflammatory diseases.^{16,36,37} Recent research has also demonstrated that age-related changes in circadian rhythmicity have major consequences on innate immunity.³⁸ Macrophages are the first line of defense against bacterial infections, and their function is controlled strongly by the circadian clock.^{31,38–41} Interestingly, it has been reported that circadian transcription and rhythmicity of phagocytosis are impaired in

aged peritoneal macrophages.³⁸ In the present study, we investigated the link between age-related circadian clock dysfunction in the lungs and altered anti-bacterial defenses in the mouse. Our results identify the nuclear receptor Rev-erb- α as the main clock component altered during aging and as a potential therapeutic target for infections in older adults.

RESULTS

Aging alters time-of-day control in pulmonary immune defenses against pneumococcal infection

It is still not known whether time-of-day susceptibility to pulmonary infection is altered in aged individuals. We first sought to determine whether host defenses against *S. pneumoniae* in young-adult mice (2 months old) displayed daily oscillations. To this end, we used *S. pneumoniae* serotype 1, an invasive serotype that induces pneumonia and bacteremia.⁴² Young-adult mice were intranasally infected at zeitgeber time 0 (ZT0), ZT6, ZT12, and ZT18, and the numbers of live pneumococci were determined 24 h post infection. As assessed by lung bacterial burden, the young-adult mice were significantly more susceptible to infection at ZT6 and ZT12 (the middle and end of the rest phase, respectively) than at ZT0 and ZT18 (Figure 1A, middle). Invasive disease, assessed by splenic dissemination of bacteria, was likewise more elevated at ZT6 and ZT12 than at ZT0 and ZT18 (Figure 1A, right). For the rest of the study, we focused on the two opposing time points ZT0 (when young-adult mice are less susceptible to infection) and ZT12 (when young-adult mice are more susceptible to infection). We next assessed the impact of aging on circadian host defenses in 22-month-old mice (considered to be equivalent to 70-year-old humans⁴³ and referred to hereafter as “elderly mice”). Relative to their young counterparts, elderly mice were significantly more susceptible to infection at ZT0 (Figure 1B). Strikingly, the time-of-day difference in susceptibility to infection observed in young-adult mice was not observed in elderly mice.

We then determined whether perturbations in host defense rhythmicity in elderly mice are associated with altered variations in immune cell counts in the lungs at ZT0 and ZT12. We particularly focused on cell types known to be critical in the early step of host defense against pneumococcal infection including alveolar macrophages (AMs), neutrophils, and non-conventional T lymphocytes.^{44–47} Flow-cytometry analysis revealed major differences between naive (no infection) young-adult mice and elderly mice. In young-adult mice, the absolute cell counts of AMs were

Figure 1. Loss of the time-of-day control in pulmonary anti-pneumococcal defense, lung cellularity, and reactivity to Toll-like receptor agonists in elderly mice

- (A) Young-adult mice were infected with *S. pneumoniae* at ZT0 (i.e., at lights-on time), ZT6, ZT12 (lights-off time), or ZT18.
 - (B) Young-adult mice and elderly mice were infected at ZT0 and ZT12 with *S. pneumoniae*. The number of bacteria in the lungs and spleen was determined 24 h post infection. A pool of two independent experiments is depicted (A, $n = 16$; B, $n = 14–17$).
 - (C) Lungs from naive young-adult and elderly mice were collected at ZT0 and ZT12 and analyzed by flow cytometry. SSC^{low}CD45⁺ cells were analyzed. The absolute number of AMs (CD11c⁺SiglecF⁺CD11b⁻), monocytes (CD11b⁺Ly6C⁺), and neutrophils (CD11b⁺Ly6G^{hi}) per lungs are represented ($n = 4–5$). One representative experiment out of three is shown.
 - (D) Lung cells (2×10^5 /well) from naive young-adult and elderly mice were exposed to LPS (1 ng/mL), R848 (10 μ g/mL), or CpG ODNs (10 μ g/mL) for 24 h. IL-12p40 and IFN- γ in supernatants were quantified by ELISA ($n = 3–7$). One representative experiment out of two is shown.
- Each dot represents one mouse. Except for determination of the bacterial load (A and B) where the bar represents the median, all graphs show mean \pm SEM. Significant differences were determined using the non-parametric Kruskal-Wallis test corrected with Dunn's test for multiple comparisons (A) or using two-way ANOVA followed by Tukey's post hoc test (B–D). * $p < 0.05$, ** $p < 0.01$, *** $p < 0.001$, **** $p < 0.0001$.

higher at ZT0 than at ZT12, whereas there were no significant changes for other immune cells examined (Figures 1C and S1). Remarkably, the rhythmicity of AM numbers observed in young-adult mice was not significant in elderly mice, while the number of monocytes and neutrophils became rhythmic (for the latter, cell count was higher at ZT12 than at ZT0) (Figure 1C). It is noteworthy that the same phenomenon (significant rhythmicity in aged lungs) occurred for dendritic cells and CD4⁺ T cells (Figure S1). Rapid cytokine production in response to an infectious challenge is critical for lung defenses. In line with the results shown in Figure 1A (higher resistance at ZT0), lung cells from young-adult mice produced high amounts of cytokines (IL-12p40 and interferon- γ [IFN- γ]) at ZT0 in response to lipopolysaccharide (LPS), resiquimod (R848), and CpG oligodeoxynucleotides (CpG ODNs) (Figure 1D). In contrast, except for IL-12p40 production in response to R848, no significant ZT0 vs. ZT12 differences in cytokine release were seen in elderly mice. Overall, altered time-of-day control in pulmonary immune defenses in elderly mice was associated with lower daily variations in basal AM counts and cytokine production levels.

Aging alters the pulmonary circadian transcriptome, with the clock component Rev-erb- α being the most impaired

We next looked at whether alteration of the time-of-day difference in pulmonary immune defenses against pneumococcal infections in elderly mice was associated with changes in time-of-day variations in gene expression. To this end, we compared the circadian transcriptome in lungs collected from infection-naive young-adult and elderly mice at ZT0, ZT4, ZT8, ZT12, ZT16, and ZT20. A rhythmicity analysis incorporating non-parametric methods (RAIN)⁴⁸ revealed that 2,818 transcripts were rhythmic in both young-adult and elderly mice (adjusted p value <0.05) (Figure 2A). Interestingly, a set of 3,740 transcripts was rhythmic in young-adult mice only, while another set of 2,895 transcripts was rhythmic in elderly mice only. Enrichment analysis of gene ontology (GO) biological processes indicated that pathways found to be rhythmic in young-adult mice (such as “proteostasis,” “leukocyte migration,” and “apoptosis”) were not rhythmic in elderly mice (Figure S2A). In contrast, some GO terms (including “cilium functions” and “hemostasis”) became rhythmic in elderly mice (Figure S2B). These results suggest that the rhythmic transcriptome in the lungs is reprogrammed in elderly animals. Rhythmically expressed genes in both young-adult and elderly groups were in “matrix remodeling,” “kinase activity,” and “epithelial/endothelial functions” GO pathways (Figure S2C). GO pathways related to immune functions (including “leukocyte migration” and “adaptive immunity”) were specifically enriched in young-adult mice (Figure S3A). In contrast, no specific GO terms related to immune functions were enriched in elderly mice. Importantly, rhythmic genes involved in immune responses (including macrophage functions such as “phagocytosis” and “ROS metabolism”) were observed in the lungs from young-adult and elderly mice (Figure S3B). We therefore hypothesized that peak expression, namely acrophase, of rhythmically expressed genes, including those involved in immune responses, may be shifted between young-adult and elderly mice in the lung. Most circadian genes reached their acrophase

at ZT4 and ZT16 in young-adult mice and at ZT0 and ZT8 in elderly mice (Figure 2B). This observation suggested that the enriched GO terms might be different at specific time points. Indeed, some GO terms were time shifted in lungs from elderly mice relative to lungs from young-adult mice. Importantly, genes involved in the control of the circadian clock were enriched at opposing time points in young-adult mice (ZT4) and elderly mice (ZT16). This shift might contribute to the overall impairment in diurnal gene expression observed in lungs from elderly mice. Furthermore, GO terms related to “phagocytosis” were advanced by 4 h in lungs from elderly mice relative to lungs from young-adult mice. Terms related to “macrophage migration and activation” were enriched only in young-adult mice (at ZT4 and ZT8, respectively) (Figure 2B). In contrast, terms related to “glucocorticoid receptor signaling” (stress-associated pathways involved in the control of inflammation and immune suppression⁴⁹) were enriched at ZT0 and ZT16 in elderly mice. We next sought to identify genes whose daily pulmonary expression is altered by aging. For this purpose, we compared lung transcript expression at ZT0 and ZT12 in lungs from young-adult mice and elderly mice. A principal-component analysis (PCA) revealed four distinct groups based on age and time-of-day conditions (Figure 2C). We next performed a differential analysis of the interaction between age and time-of-day variables by using the galaxy-based tool for interactive analysis of transcriptomic data (GIANT).⁵⁰ We identified 12 genes whose daily expression between ZT0 and ZT12 was influenced by age ($p < 0.01$) (Figure 2D). Strikingly, while pulmonary *Nr1d1* (encoding the clock component Rev-erb- α) expression displayed a robust rhythmicity in young-adult mice (higher at the end of the rest period), its expression was always high in elderly mice (false discovery rate [FDR] < 0.1). This is particularly interesting because Rev-erb- α is a key transcription factor that controls lung immunity and inflammation.^{8,11,12} This finding was confirmed by RT-qPCR (Figure 2E). It is noteworthy that the basal level of *Nr1d1* transcripts was high in aged lungs at ZT0, i.e., the time point corresponding to blunted expression in young adults. Altogether, these data show that the impaired circadian defense in elderly mice was associated with changes in the circadian transcriptome, the clock component and nuclear receptor Rev-erb- α being the most affected gene.

Rev-erb- α antagonism protects against pneumococcal infection, in part by activating the phagocytic and bactericidal activities of alveolar macrophages

While the role of Rev-erb- α in inflammation and innate immunity has been well characterized,^{12,14,19} its potential role in lung defense against infection is more elusive. To address this issue, Rev-erb- α -deficient (*Nr1d1*^{-/-}) and Rev-erb- α -proficient (*Nr1d1*^{+/+}) young-adult mice were infected with *S. pneumoniae* at ZT12 (i.e., a ZT at which the pulmonary expression of Rev-erb- α protein is high¹²). Compared with littermate controls, *Nr1d1*^{-/-} mice were more resistant to pneumococcal infection (Figure 3A). To determine whether Rev-erb- α pharmacological modulation affects susceptibility to pneumococcal infection, we performed experiments in which the Rev-erb agonist SR9009 or antagonist SR8278 was given before infection. To avoid systemic metabolic impairments (e.g., lipolysis and body

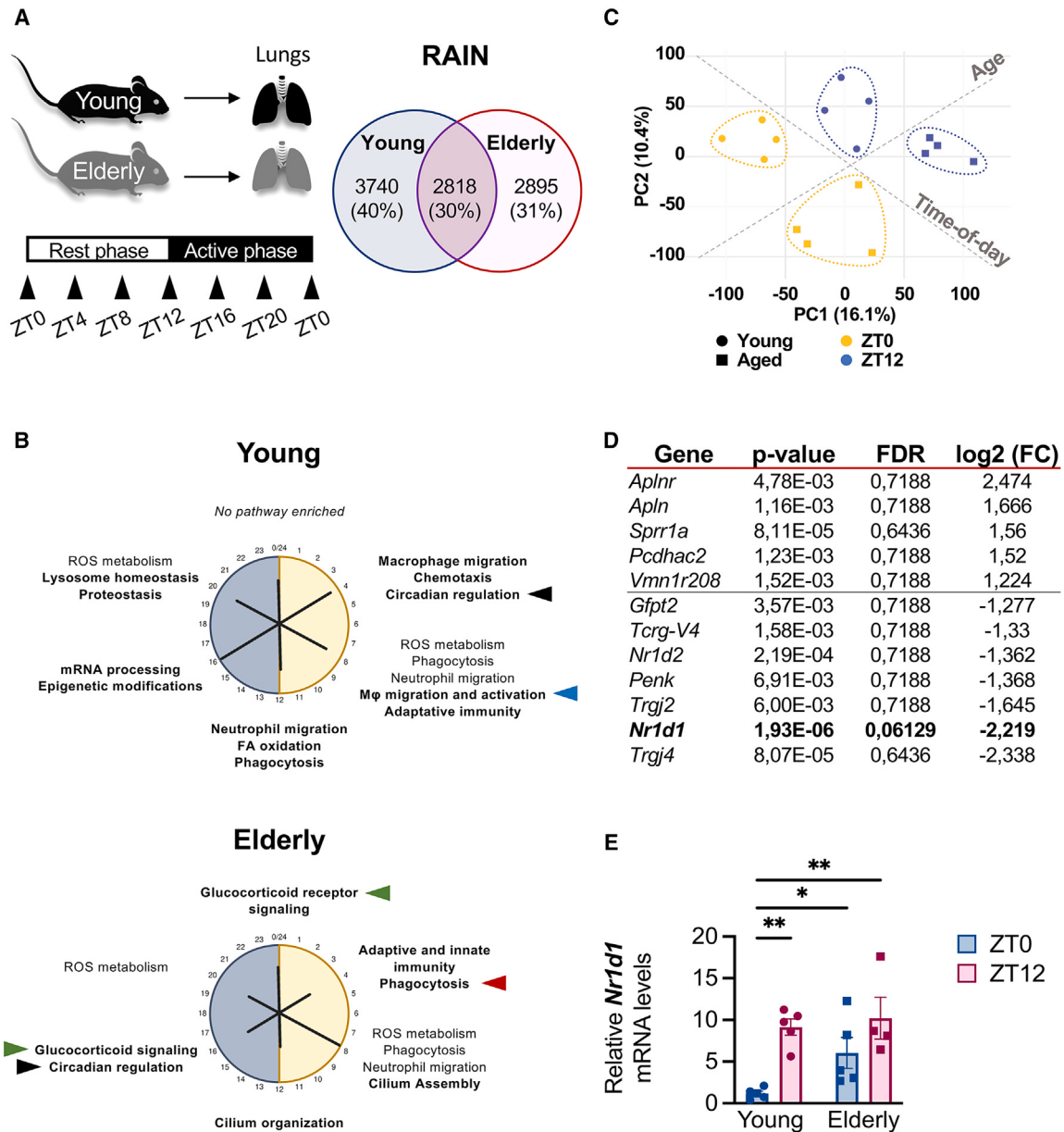


Figure 2. Altered rhythmicity of circadian transcriptome and Rev-erb- α transcript expression in aged lungs

(A) (Left) Design of the transcriptomic experiment. Lungs from young-adult and elderly mice were harvested every 4 h over 24 h, and RNAs were sequenced. (Right) Venn diagram of the rhythmically expressed genes in young-adult mice, elderly mice, and both age groups.

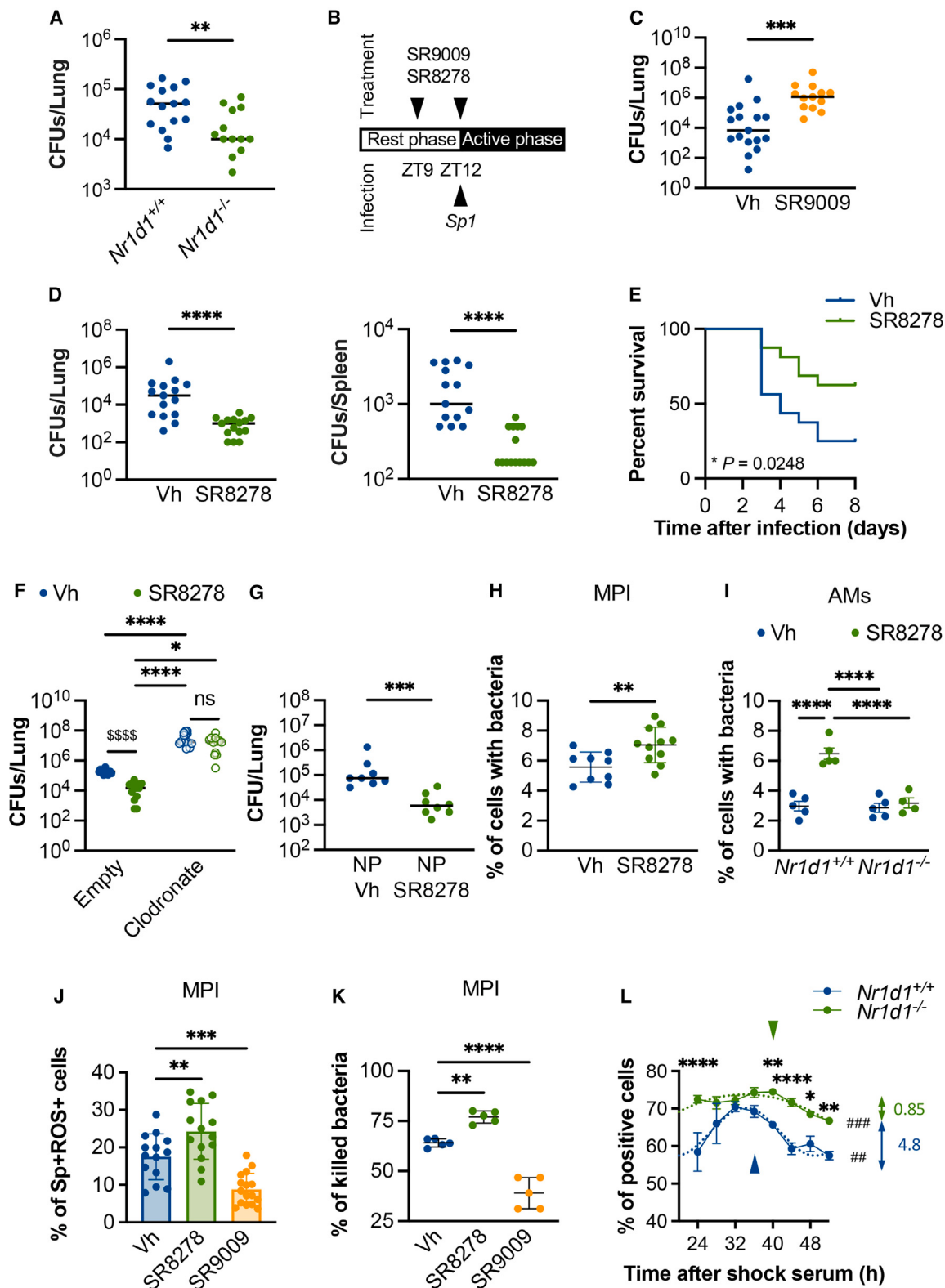
(B) Peak time maps of oscillatory GO terms from young-adult lungs and old lungs (adjusted p values <0.05). The length of the transversal bars within the circles is proportional to the number of circadian genes. Bold typeface indicates pathways specific to young-adult lungs or to old lungs. Arrowheads point to phase-shifted pathways. For clarity, GO terms relevant to our study are depicted.

(C) Principal-component (PC) analysis showing the distinct separation of young-adult and elderly groups and ZT0 and ZT12 groups. Plain circles, young-adult mice; squares, elderly mice; yellow, ZT0; blue, ZT12. Gray dashed lines distinguish ZT0 from ZT12 groups (“Time-of-day” line) and young-adult from elderly mice (“Age” line).

(D) Differential analysis revealing genes whose diurnal regulation is altered during aging (considering interaction between age and time-of-day variables). Genes with a p value <0.05 as well as genes with a false discovery rate (FDR) <0.1 are shown.

(E) *Nr1d1* transcript expression levels in lungs from young-adult and aged lungs at ZT0 and ZT12. Data are expressed as the fold change relative to average gene expression in young-adult lungs (ZT0). Each dot represents one mouse ($n = 4-5$).

All graphs show mean \pm SEM. Significant differences were determined using two-way ANOVA followed by Newman-Keuls post hoc test for multiple comparisons. * $p < 0.05$, ** $p < 0.01$.



(legend on next page)

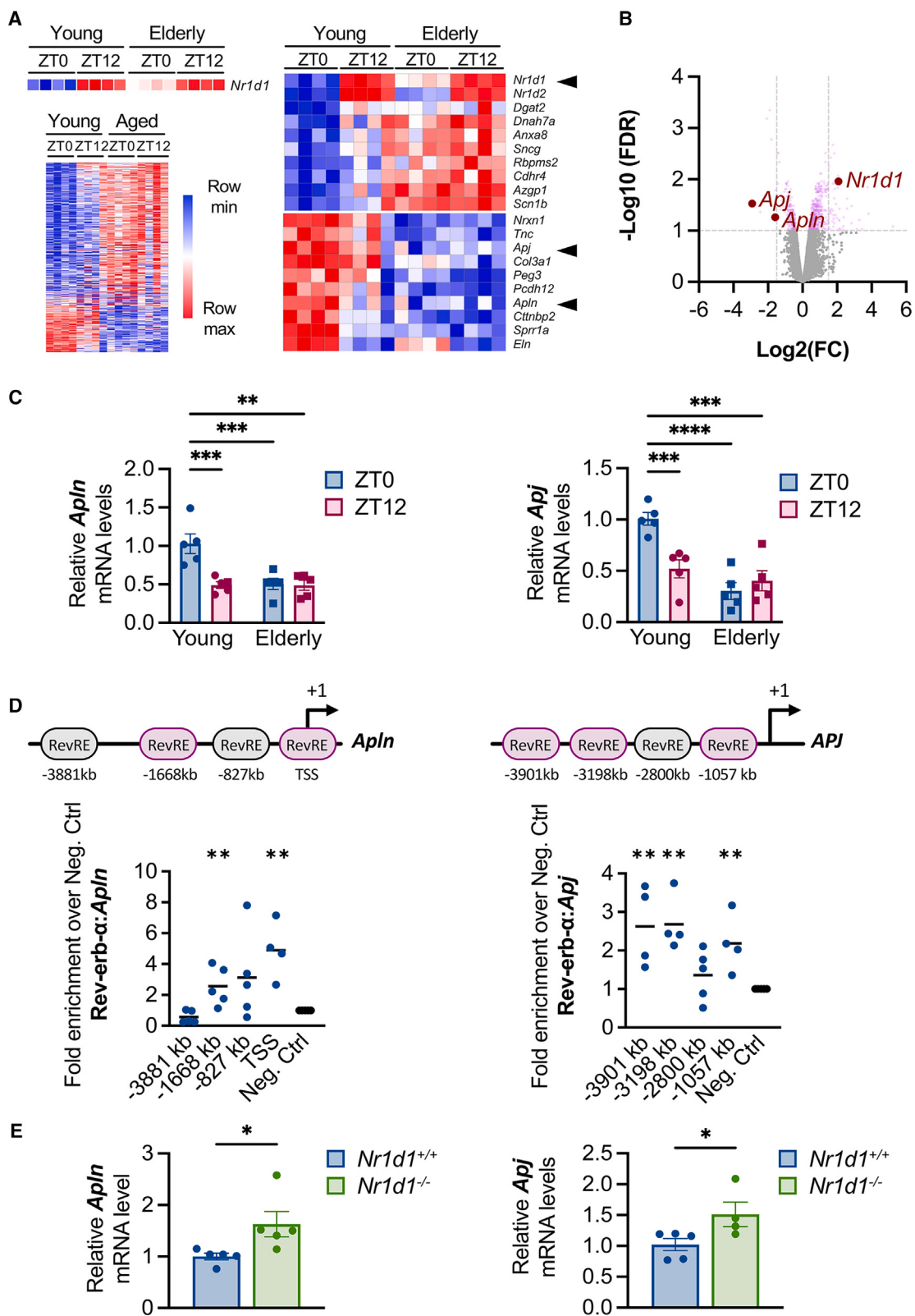
weight loss^{51,52}), SR9009 or SR8278 were administered intranasally at ZT9 (i.e., 3 h before infection) and ZT12 (Figure 3B). The SR9009-treated mice exhibited a significantly higher bacterial count in the lungs compared with vehicle-treated mice (Figure 3C). SR8278 is known to block Rev-erb- α repressive transcriptional activity and produces an increase in Rev-erb- α target gene expression.^{21,53} Indeed, treatment with SR8278 effectively reduced *Nr1d1* expression and induced *Arntl* (encoding *Bmal1*) expression in the lungs (Figure S4A). Interestingly, compared with the vehicle control, treatment with SR8278 resulted in greater resistance against pneumococcal infection (Figure 3D). The protective effect of SR8278 was not evidenced in *Nr1d1*^{-/-} mice (Figure S4B). At 36 h post infection, the protective effect was still observed in terms of pulmonary and splenic bacterial loads (Figure S4C). The improved control of the infection by SR8278 treatment was associated with ameliorated survival (Figure 3E).

We then investigated mechanisms leading to SR8278-mediated protection against pneumococcal infection. Interleukin-17 (IL-17) production by non-conventional T lymphocytes, including $\gamma\delta$ T lymphocytes, is important in the early recruitment of neutrophils in lung tissue.⁴⁷ SR8278 did not significantly modulate the numbers of IL-17-expressing $\gamma\delta$ T lymphocytes and neutrophils in infected lungs (Figure S4D). The intracellular expression of IFN- γ by neutrophils, known to facilitate bacterial clearance,⁴⁵ was not modulated by SR8278 (data not shown). AMs are the major gatekeepers of the pulmonary alveolus, where they phagocytose and kill pathogenic bacteria including *S. pneumoniae*.⁴⁴ Airway administration of clodronate liposomes is known to deplete AMs (but not neutrophils⁴⁷). As expected, clodronate liposome augmented the number of bacteria in the lungs (Figure 3F). Interestingly, clodronate liposomes completely blocked the protective effects of SR8278. As clodronate liposomes also affect other cell types such as dendritic cells,⁵⁴ these data sug-

gest a key role of AMs in SR8278-mediated protection against pneumococcal infection. To confirm this finding, SR8278 was encapsulated in biocompatible nanoparticles so that AMs were specifically targeted. Indeed, exposure to nanoparticles led to potent internalization by AMs (Figure S5A). Compared with vehicle-containing nanoparticles, treatment with SR8278-containing nanoparticles resulted in a lower bacterial load in the lungs and the spleen (Figures 3G and S5B). We then investigated the potential effect of SR8278 on the phagocytic and intracellular killing abilities of Max Planck Institute (MPI) cells (a cell line that mimics the main features of primary AMs^{55,56}). Synchronized MPI cells were treated with SR8278 in the middle of the ascending phase of Rev-erb- α expression (Figure S5C). Interestingly, *S. pneumoniae* were internalized more effectively by SR8278-treated macrophages than by vehicle-treated cells. Indeed, the number of cells harboring intracellular bacteria (Figure 3H) and the number of bacteria per cell (Figure S6A) were significantly higher when Rev-erb- α was antagonized. Confocal microscopy analysis using eGFP-expressing *S. pneumoniae* confirmed the higher phagocytic activity of macrophages after SR8278 treatment (Figure S6B). To confirm these findings in another setting, MPI cells were exposed to pHrodo Red Zymozan A bioparticle conjugates. Compared to vehicle, the phagocytic activity of MPI cells, here based on acidification of the particles as they are ingested, was enhanced by SR8278 (Figure S6C). This was not associated with enhanced expression of (endocytic) receptors known to facilitate phagocytosis³ (Figure S6D and data not shown). Importantly, SR8278 also enhanced the phagocytic activity of AMs collected from *Nr1d1*^{+/+} mice (Figures 3I and S6E). In contrast, it failed to do so in *Nr1d1*^{-/-} AMs, confirming the Rev-erb- α -dependent action of SR8278 on phagocytosis. This finding was confirmed using synchronized bone-marrow-derived macrophages (BMDMs) (Figure S6F). The early generation of reactive oxygen species

Figure 3. Role of Rev-erb- α and alveolar macrophages in host defense against *S. pneumoniae* infection

- (A–D) (A) *Nr1d1*^{-/-} and *Nr1d1*^{+/+} mice were infected with *S. pneumoniae* at ZT12. As illustrated in (B), wild-type mice were treated by the intranasal route with SR9009 (25 mg/kg) (C) or with SR8278 (25 mg/kg) (D) at ZT9 and ZT12 and then infected with *S. pneumoniae* at ZT12. The number of bacteria was determined 24 h post infection. A pool of two experiments is depicted (A, $n = 13$ –15; C, $n = 13$ –17; D, $n = 15$).
- (E) Mice were treated with vehicle (Vh) or SR8278 and then infected with *S. pneumoniae*. Survival of mice was monitored daily ($n = 16$, pool of two separate experiments).
- (F) Mice were intranasally treated with empty liposomes or clodronate liposomes (50 μ L/mouse). Twenty-four hours later, animals were treated with vehicle (Vh) or SR8278 and then infected (as in D) ($n = 12$ –14, pool of two separate experiments).
- (G) Mice were inoculated by the intranasal route with SR8278 vectorized in NPs (3.4 mg/kg) at ZT9 and ZT12. Mice were infected with *S. pneumoniae* at ZT12. One representative experiment out of two is shown ($n = 8$).
- (H) Synchronized MPI cells were exposed to vehicle (Vh) or SR8278 (2 μ M) for 1 h and then to eGFP *S. pneumoniae* (MOI 10) for 2 h. Shown is the percentage of cells with bacteria ($n = 9$ –11, pool of two separate experiments).
- (I) AMs were collected from the bronchoalveolar lavages of young-adult *Nr1d1*^{+/+} or *Nr1d1*^{-/-} mice. Cells were then treated with vehicle (Vh) or SR8278 (2 μ M) for 1 h and exposed to *S. pneumoniae* (MOI 10) for 2 h. Shown is the percentage of cells with bacteria ($n = 4$ –5).
- (J) MPI cells were treated as in (H) and then exposed to *S. pneumoniae* (MOI 10) for 4 h. The frequency of MPI cells having internalized eGFP-*S. pneumoniae* and producing ROS is indicated ($n = 14$ –16, pool of two separate experiments).
- (K) MPI cells were exposed to vehicle (Vh), SR8278 (2 μ M), or SR9009 (2 μ M) for 1 h and then to live *S. pneumoniae* (MOI 10). The percentage of killed bacteria was calculated 5 h post infection ($n = 5$).
- (L) Synchronized *Nr1d1*^{+/+} or *Nr1d1*^{-/-} BMDMs were assayed for phagocytosis of pHrodo Red Zymozan A bioparticle conjugates over a 28-h period. Statistical differences between *Nr1d1*^{+/+} and *Nr1d1*^{-/-} are indicated for each time point (two-way ANOVA followed by a Sidak post hoc test). Arrowheads indicate the acrophase. The amplitudes of rhythmicity are indicated. A cosinor analysis was performed and visualized by the dashed line. Statistical analysis of the rhythmicity was performed using JTK_Cycle (# $p < 0.01$, # $p < 0.001$) ($n = 6$).
- In (A), (C), (D), (F), and (G), each dot represents one mouse (the bar represents the median). Graphs show mean \pm SD (H, J, and K) or mean \pm SEM (I and L). Significant differences were determined using the Mann-Whitney U test (A, C, D, G, and H), the log-rank test (E), or two-way ANOVA followed by Tukey's post hoc test for multiple comparisons (F, I, and L) or one-way ANOVA followed by Dunnett's post hoc test (J and K). * $p < 0.05$; ** $p < 0.01$, *** $p < 0.001$, **** $p < 0.0001$.



(legend on next page)

(ROS) by macrophages (during the oxidative burst) contributes to bactericidal activity.⁵⁷ Interestingly, SR8278 enhanced the percentage of *S. pneumoniae*-positive, ROS-producing AMs while SR9009 had the opposite effect (Figures 3J and S6G). Relative to Rev-erb- α -proficient macrophages, the percentage of *S. pneumoniae*-positive, ROS-producing *Nr1d1*^{-/-} macrophages was significantly enhanced (Figure S6H). We then assessed the effect of SR8278 treatment on the bactericidal activity of macrophages. Treatment of MPI cells with SR8278 significantly enhanced the killing of *S. pneumoniae*, while SR9009 had the opposite effect (Figure 3K).

To investigate the putative role of Rev-erb- α in circadian phagocytosis of macrophages, synchronized BMDMs generated from *Nr1d1*^{+/+} and *Nr1d1*^{-/-} mice were exposed to pHrodo Red Zymozan A bioparticle conjugates at 4-h time intervals over a 28-h period. As expected,³⁶ measurement of the percentage of cells that ingested the particles shows that *Nr1d1*^{+/+} macrophages display a circadian phagocytic activity ($p = 0.0011$ by JTK_Cycle, acrophase 36 h post synchronization, amplitude 4.8) (Figure 3L). In addition, the intracellular particle load per cell clearly showed circadian variation ($p = 0.0033$, acrophase 36 h post synchronization, amplitude 1,793) (Figure S6I). Interestingly, the acrophase of the phagocytic activity corresponds to the nadir of *Nr1d1* expression in synchronized cells (Figure S6J), suggesting that Rev-erb- α might inhibit phagocytosis. Indeed, *Nr1d1*^{-/-} cells displayed higher phagocytic activity relative to *Nr1d1*^{+/+} macrophages (Figures 3L and S6I). Importantly, *Nr1d1*^{-/-} macrophages displayed an altered rhythmicity of percentage of cells with internalized particles ($p = 0.00099$, acrophase 40 h post synchronization, amplitude 0.85) (Figure 3L), while the rhythmicity of the particle load per cell was abolished in *Nr1d1*^{-/-} cells ($p = 0.68$, acrophase 40 h post synchronization, amplitude 0.25) (Figure S6I). These findings emphasize the key role of Rev-erb- α in the control of circadian macrophage phagocytosis and demonstrate that antagonizing the Rev-erb- α activity enhances the phagocytosis and bactericidal activity of AMs, a process involved in protection against pneumococcal infection.

***Apln* and *Apj* are new Rev-erb- α target genes differentially regulated during aging**

To gain insights into mechanisms potentially involved in SR8278-mediated protection, we sought to characterize Rev-erb- α target genes, focusing on those having altered circadian rhythmicity during aging. To this end, we performed a clustering of genes based on the *Nr1d1* expression profile (ZT0 and ZT12) (Figure 4A). In line with the GIANT interaction analysis (Figure 2D),

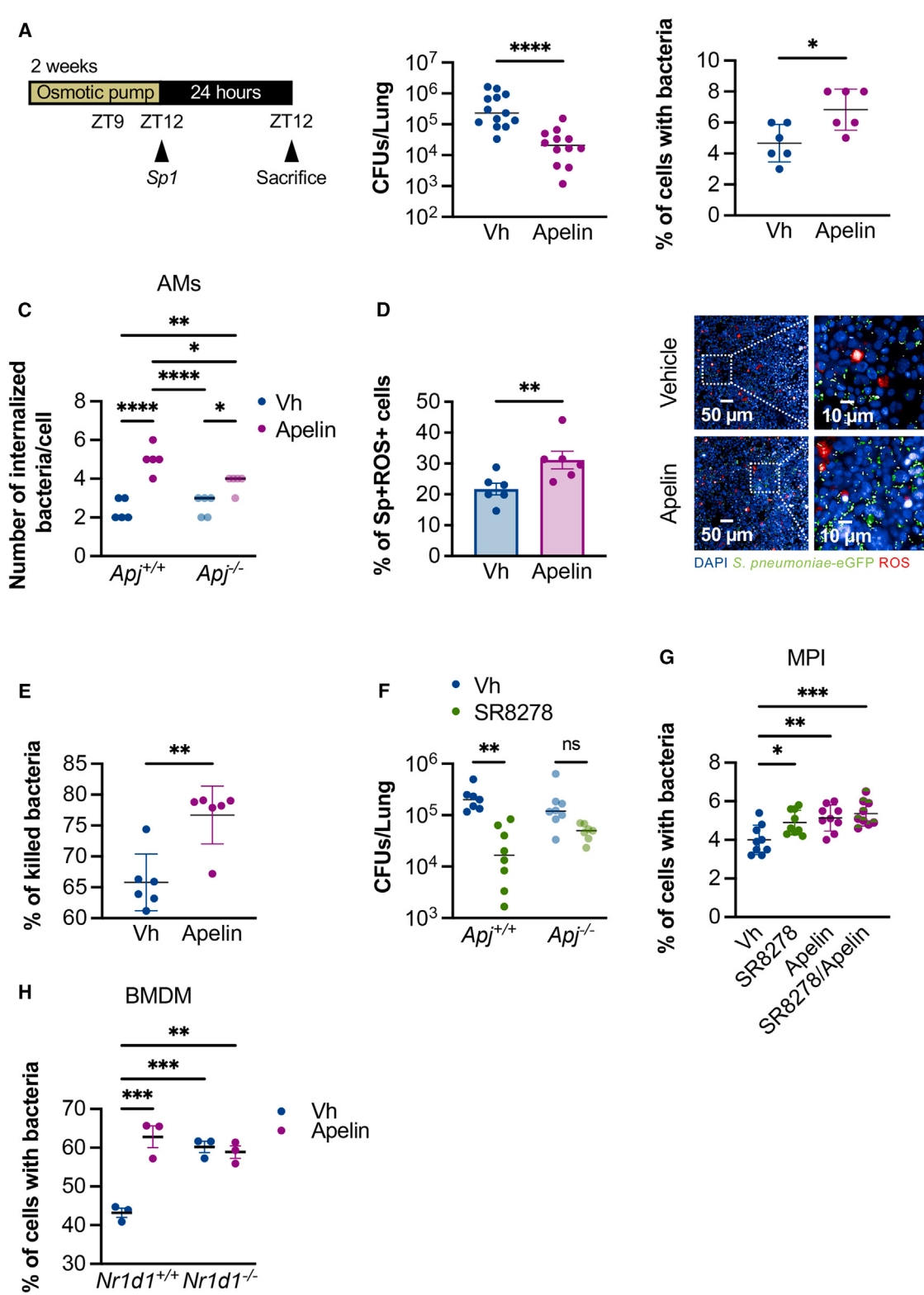
genes with opposing profiles included *Apln* (coding for apelin) and *Apj* (coding for the apelin receptor, APJ). The apelin pathway is known to regulate many physiological and pathological mechanisms and is a target for the maintenance of health during old age.^{58–62} Interestingly, *Apln* and *Apj* were among the most strongly downregulated genes in elderly mice (Figure 4B). RT-qPCR revealed that the daily variation in the expression of *Apln* and *Apj* mRNAs was absent in lungs from elderly mice (Figure 4C). Given that (1) Rev-erb- α and *Apln/APJ* display anti-phase expression in lungs from young-adult mice and (2) Rev-erb- α is a transcriptional repressor, we looked at whether Rev-erb- α might directly control the expression of *Apln* and *Apj* by binding to their promoters. An *in silico* analysis revealed the presence of a putative consensus response element (RevRE) in the *Apln* and *Apj* promoters (Figure 4D, upper). To determine whether Rev-erb- α was recruited to *Apln* and *Apj* promoters, we performed a chromatin immunoprecipitation (ChIP) assay on lungs from young-adult mice. Rev-erb- α was recruited at different RevREs within the *Apln* promoter ($-1,668$ kb, transcription start site), the *Apj* promoter ($-3,901$ kb, $-3,198$ kb, and $-1,057$ kb), and the *Arntl* promoter (positive control) (Figures 4D [lower] and S7A). In line with the repressive activity of Rev-erb- α , H₃K₂₇me3, a transcriptional inactivation mark, was increased at RevRE in *Apln*, *Apj*, and *Arntl* (positive control) promoters (Figures S7B–S7D). Accordingly, and compared to wild-type mice, the transcript expression levels of *Apln* and *Apj* were augmented in the lungs from *Nr1d1*^{-/-} mice (Figure 4E). These results demonstrate that Rev-erb- α binds to the *Apln* and *Apj* promoters to functionally control their expression, thus identifying these genes as new Rev-erb- α target genes.

The Rev-erb- α /APJ pathway plays a role in pulmonary defense against pneumococcal infection

As Rev-erb- α antagonism protects against pneumococcal infection (Figure 3D), we reasoned that activation of APJ upon Rev-erb- α inhibition may upregulate pulmonary defenses against *S. pneumoniae*. We first investigated the effect of apelin administration on the bacterial load. Since apelin has a short half-life,⁶³ we used osmotic pumps to continuously deliver the peptide. Interestingly, apelin treatment significantly reduced the pneumococcal burden in the lungs (Figure 5A). Although APJ is known to be functional in peritoneal macrophages,⁶⁴ its potential role in AMs has yet to be studied. Pretreatment of synchronized MPI cells with apelin resulted in higher levels of phagocytosis (Figures 5B and S8A). Apelin also enhanced the phagocytosis of AMs collected from *Apj*^{+/+} mice (Figure 5C). The percentage

Figure 4. *Apln* and *Apj* as new Rev-erb- α target genes

- (A) (Left) Heatmap of *Nr1d1* mRNA pattern in the different groups (microarray analysis). (Right) Heatmap of top ten genes clustered with *Nr1d1* and heatmap of top ten genes with a profile opposite to that of *Nr1d1*.
- (B) Volcano plot shows significantly upregulated and downregulated genes between young-adult lungs and aged lungs (ZT0). The horizontal line represents the FDR at 0.1.
- (C) *Apln* and *Apj* transcript expression levels in lungs from young-adult and aged lungs at ZT0 and ZT12. Each dot represents one mouse ($n = 4–5$).
- (D) (Upper) Schemes represent putative Rev-erb response elements in *Apln* and *Apj* promoters unveiled by *in silico* analysis using Promoter DataBase. (Lower) ChIP analysis of Rev-erb- α occupancy to the *Apln*, *Apj*, and *Arntl* (positive control) promoters. TSS, transcription start site ($n = 4–5$).
- (E) *Apln* and *Apj* transcript expression levels in lungs from young-adult *Nr1d1*^{+/+} and *Nr1d1*^{-/-} mice (collected at ZT8). Each dot represents one mouse ($n = 5$). Except for the ChIP experiment (D) where the bar represents the mean, all graphs show mean \pm SEM. Significant differences were determined using two-way ANOVA followed by Newman-Keuls post hoc test for multiple comparisons (C and D) or using Mann-Whitney U test (E). * $p < 0.05$, ** $p < 0.01$, *** $p < 0.001$, **** $p < 0.0001$.



(legend on next page)

of *S. pneumoniae*-positive, ROS-producing macrophages was augmented upon apelin treatment (Figure 5D). Lastly, relative to vehicle, apelin treatment significantly enhanced the bactericidal activity of macrophages (Figure 5E). Hence, the apelin/APJ signaling pathway is relevant in macrophage-dependent bacterial killing. We then looked at whether the SR8278-mediated protection against pneumococcal infection depended on APJ. To this end, we evaluated the *in vivo* effect of SR8278 in *Apj*^{+/+} and *Apj*^{-/-} mice. SR8278 administration was associated with a significantly lower bacterial load in *Apj*^{+/+} mice but not in *Apj*^{-/-} mice (Figure 5F). In line with this, relative to SR8278 alone, the combination of apelin with SR8278 strengthens the phagocytic and killing activities of MPI cells (Figures 5G, S8B, and S8C). *Nr1d1*^{+/+} and *Nr1d1*^{-/-} BMDMs were then exposed to apelin. Apelin increased the phagocytic activity of *Nr1d1*^{+/+} macrophages to reach the activity of *Nr1d1*^{-/-} macrophages, while it did not further increase the phagocytic level of *Nr1d1*^{-/-} macrophages (Figure 5H). This latter finding highlights the role of Rev-erb- α in apelin-mediated phagocytosis. We conclude that the Rev-erb- α /APJ pathway might be important in pulmonary defense against pneumococcal infection.

Rev-erb- α antagonism protects against pneumococcal infection in elderly mice

Unbiased transcriptomic analysis and pharmacological studies in young-adult mice suggested that Rev-erb- α and APJ are potential targets for enhancing pulmonary defenses in elderly mice. We first sought to establish whether Rev-erb- α antagonism can reduce the bacterial load in elderly mice. Intranasal SR8278 inoculation at ZT9 and ZT12 significantly lowered the bacterial load in elderly mice (Figure 6A). Excessive neutrophil levels in *S. pneumoniae*-infected aged lungs are associated with deleterious outcomes.^{65–67} Compared to the vehicle control group, the number of neutrophils was not significantly affected in SR8278-treated mice (slightly reduced) (Figure 6B, left). Consistent with this, SR8278 treatment did not influence the mRNA levels of the known neutrophil chemoattractants chemokine ligand 1 (CXCL1) and chemokine ligand 2 (CCL2) (Figure 6B,

right). Lastly, we looked at whether APJ signaling is associated with better protection in elderly mice. Apelin treatment failed to further enhance the protective effect of SR8278 (Figure 6C, middle), perhaps because the level of APJ protein in aged lungs remained unchanged in response to SR8278 (Figure S9). It is noteworthy that SR8278 and SR8278 plus apelin lowered bacterial dissemination (Figure 6C, right). In summary, APJ signaling alone is relevant for pulmonary defenses in young-adult mice, but Rev-erb- α antagonism is sufficient to protect elderly mice against pneumococcal infections.

DISCUSSION

Even though impaired circadian rhythmicity in older adults has a major impact on many diseases and the body's immune responses,^{68,69} the potential contribution of age-mediated circadian misalignment to infection has not previously been investigated. In line with the literature data,^{11,26,27} susceptibility to pneumococcal infection was diurnally regulated in young-adult mice. Indeed, these animals were most susceptible at ZT6 and ZT12, which correspond respectively to the middle and end of the rest phase. In contrast, the diurnal control of pneumococcal infection was altered in older lungs. To firmly demonstrate this point, infection of elderly mice at four different ZTs would be necessary. In our experimental settings, a change in the time-of-day vulnerability to pulmonary infection in elderly mice was associated with lower daily variations in the number and functions of immune cells in the lungs. It is noteworthy that the cytokine response to microbial danger components was not diurnally controlled in lungs from elderly mice. The circadian transcriptome is known to change with age,^{70,71} and the lung is no exception.⁷² We established a time-domain map of GO terms enriched in the basal circadian transcriptome of lungs from young-adult mice and elderly mice; this map revealed that some GO terms present in lungs from young-adult mice were absent in lungs from elderly mice. Interestingly, the GO term "phagocytosis" was phase shifted in lungs from elderly mice. This is consistent with the suggestion by Wolff et al.⁷² that impaired rhythmicity

Figure 5. Role of APJ signaling and effect of SR8278 on pulmonary defense in young-adult mice

- (A) (Left) Alzet micro-osmotic pumps were inserted subcutaneously in young-adult mice, delivering 0.11 μ L (0.055 μ g) apelin per hour for 14 days. Fourteen days later, mice were infected with *S. pneumoniae* at ZT12. (Right) The number of bacteria in lungs is depicted (24 h post infection) ($n = 12–13$, pool of two independent experiments).
 - (B) Synchronized MPI cells were exposed to apelin (5 μ g/mL) for 1 h and then to eGFP *S. pneumoniae* (MOI 10) for 2 h. Shown is the percentage of cells with bacteria ($n = 6$, pool of two experiments).
 - (C) AMs were collected from the bronchoalveolar lavages of young-adult *Apj*^{+/+} or *Apj*^{-/-} mice. Cells were then treated with vehicle (Vh) or apelin (5 μ g/mL) for 1 h and then exposed to *S. pneumoniae* (MOI 10) for 2 h. Shown is the number of bacteria per cell ($n = 5$).
 - (D) The frequency of MPI cells having internalized eGFP-*S. pneumoniae* and producing ROS is indicated ($n = 6$, pool of two experiments). Representative images are depicted on the right.
 - (E) Synchronized MPI cells were exposed to apelin (5 μ g/mL) for 1 h and then to live *S. pneumoniae* (MOI 10). The percentage of killed bacteria was calculated 5 h post infection ($n = 6$, pool of two experiments).
 - (F) *Apj*^{+/+} and *Apj*^{-/-} mice were treated with SR8278 (25 mg/kg) at ZT9 and ZT12 and then infected with *S. pneumoniae* at ZT12. The number of bacteria was determined 24 h post infection ($n = 7–8$, a representative experiment out of two).
 - (G) Synchronized MPI cells were exposed to SR8278 (2 μ M) alone, apelin (5 μ g/mL) alone, or the combination of both for 1 h. Cells were then exposed to *S. pneumoniae* for 2 h. Shown is the percentage of cells with bacteria ($n = 9–10$, pool of two experiments).
 - (H) Synchronized BMDMs generated from *Nr1d1*^{+/+} and *Nr1d1*^{-/-} mice were exposed to vehicle (Vh) or apelin (5 μ g/mL) for 1 h and then to eGFP-expressing *S. pneumoniae* (MOI 10) for 4 h. The percentage of positive cells is depicted ($n = 3$).
- Each dot represents one mouse (A, C, F, and H). Except for the determination of the bacterial load (A and F) where the bar represents the median, all graphs show mean \pm SD (B, D, E, and G) or mean \pm SEM (C and H). Significant differences were determined using the Mann-Whitney U test (A, B, D, and E) or two-way ANOVA followed by Tukey's post hoc test for multiple comparisons (C and F–H). * $p < 0.05$, ** $p < 0.01$, *** $p < 0.001$, **** $p < 0.0001$.

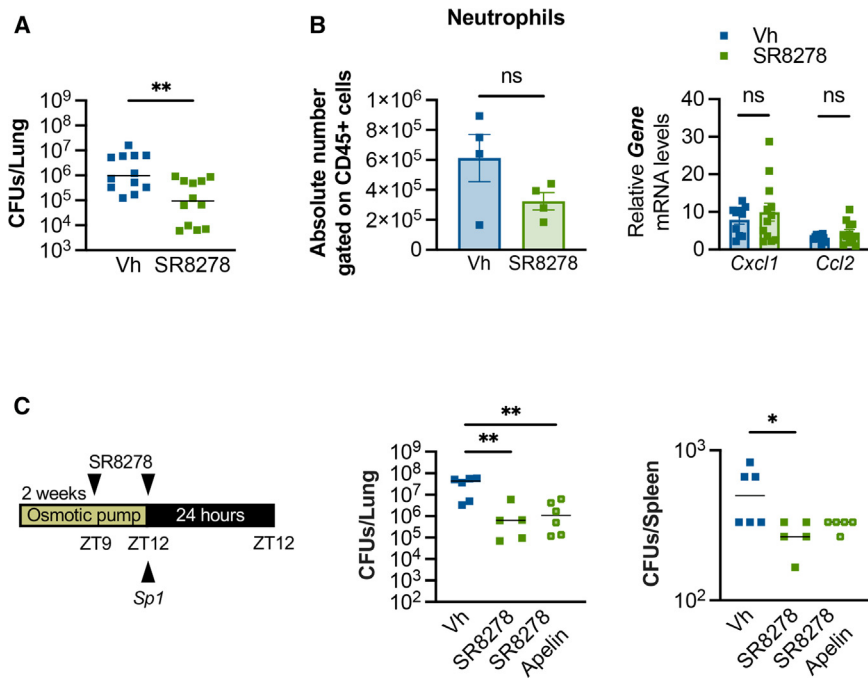


Figure 6. Effect of SR8278 on anti-pneumococcal pulmonary defense in elderly mice

(A and B) Elderly mice were treated with SR8278 (25 mg/kg) at ZT9 and ZT12 and then infected with *S. pneumoniae* at ZT12.

(A) The number of bacteria in lungs is depicted (24 h post infection) ($n = 12$, pool of two independent experiments).

(B) (Left) Absolute number of neutrophils in lungs 24 h post infection ($n = 4$, one representative experiment out of two performed). (Right) *Cxcl1* and *Ccl2* transcript expression levels in lungs. Data are expressed as the fold change relative to average gene expression in mock-infected elderly mice ($n = 8$, pool of two experiments).

(C) Fourteen days after apelin treatment, elderly mice were treated with SR8278 (25 mg/kg) at ZT9 and ZT12 and infected with *S. pneumoniae* at ZT12. The number of bacteria in lungs and spleen is depicted (24 h post infection) ($n = 5–6$, one representative experiment out of two performed). Each dot represents one mouse. The bar represents the median (A and C). Results are shown as mean \pm SEM (B). Significant differences were determined using the Mann-Whitney U test (A and B) or two-way ANOVA followed by Tukey's post hoc test for multiple comparisons (C). * $p < 0.05$, ** $p < 0.01$.

of immune gene expression in lungs from elderly mice might lead to changes in the anticipatory nature of the pulmonary response to environmental insults, including infections. Furthermore, our transcriptomic analysis revealed that processes that are not rhythmic in young-adult mice (such as “cilium functions” and “glucocorticoid signaling”) become rhythmic in elderly mice. The potential impact of these changes on the lungs’ defenses against infection has yet to be determined. It is noteworthy that the apelin pathway and the glucocorticoid pathway regulate each other. Indeed, glucocorticoids repress apelin expression, whereas apelin induces glucocorticoid signaling in various contexts.^{73,74} Furthermore, the glucocorticoid receptor represses the transcription of Rev-erb- α mRNA *in vitro* and *in vivo*,^{75,76} while Rev-erb- α physically interacts with the glucocorticoid receptor to modulate its transcriptional activity.^{77,78} In our experiments, time-of-day changes in Rev-erb- α , apelin, and APJ transcript expression were blunted in lungs from elderly mice. It remains to be formally determined whether these transcriptional changes explain the modified time-of-day vulnerability to pneumococcal infection. Nonetheless, these data prompted us to study the potential role of Rev-erb- α and the apelinergic signaling pathway in lung defenses.

Although the role of Rev-erb- α in lung function and diseases (inflammation and fibrosis) has been well described,^{12,34,78} its potential role in the lung defenses against respiratory pathogens is less clear. We addressed this question by genetic and pharmacological approaches. Our data showed that Rev-erb- α gene knockout and pharmacological inactivation of the protein enhanced host defenses against *S. pneumoniae*. This is in contrast to the study by Griepentrog et al., which identified Rev-erb- α as a key element in host protection against *Klebsiella pneumoniae* infection after exposure to blue light—a procedure

known to synchronize circadian rhythms.⁷⁹ This apparent discrepancy might be due to differences in the protocols used to stimulate or inactivate Rev-erb- α and the time-of-day treatment in particular. In our setting, mice were treated locally at the end of the rest phase (ZT9/ZT12, i.e., the peak of *Nr1d1* expression). In the study by Griepentrog et al., the mice were treated systemically at ZT6,⁷⁹ 4 h after bacterial infection. Lastly, differences might also be explained by the bacteria itself and by immune mechanisms involved in *K. pneumoniae* (gram-negative) versus *S. pneumoniae* (gram-positive) clearance. While in the study by Griepentrog et al., splenic C-C chemokine receptor 2-positive monocytes are important in protection against *K. pneumoniae* infection, AMs are critical for the protective effects of SR8278 in our setting. Our *in vitro* analysis of synchronized macrophages (MPI cells) as well as ex vivo AMs (and BMDMs) showed that Rev-erb- α inactivation upregulated, through a yet-to-be-identified mechanism, phagocytosis (and bacterial killing for MPI cells), which is in agreement with a report of reduced phagocytosis by microglia upon Rev-erb- α activation.⁸⁰ Of note, SR8278 can rescue the decreased phagocytic activity of microglia in some settings.⁸¹ Our new data are consistent and highlight the negative role of Rev-erb- α in macrophage-dependent lung defenses against bacterial (pneumococcal) infection. Hence, in addition to Rev-erb- α ’s role as a rhythmic regulator of macrophage-induced inflammation,^{14,19,20} Rev-erb- α has an essential role in phagocytosis and bacterial clearance. Importantly, we demonstrate that Rev-erb- α controls phagocytosis of macrophages in a circadian manner, at least *in vitro*. Our present results are also in line with a recent study in which circadian transcription and phagocytosis were disrupted in aged macrophages.³⁸ In the latter study, the transcription factor Kruppel-like factor 4 (encoded by a clock-controlled gene) was critical

for this process. Research on whether the loss of rhythmic expression of Kruppel-like factor 4 in macrophages is correlated with changes in Rev-erb- α expression/activity is now warranted. More generally, further investigations of the oscillatory nature of the aging program of AMs (e.g., gene expression, phagocytosis, and bactericidal activity) are likely to be very informative. Our unbiased transcriptomic analysis of lungs from elderly mice suggested a role for altered circadian apelin signaling (along with Rev-erb- α) in susceptibility to pneumococcal infection. Our data also revealed that *Apln* and *Apj* are new Rev-erb- α /APJ target genes, highlighting the potential importance of the Rev-erb- α /APJ pathway in health and disease. The apelinergic system has been linked to a number of diseases, including chronic heart failure, diabetes, inflammation, obesity, and HIV infection.⁸² Accordingly, researchers have highlighted the therapeutic potential of targeting the apelin/APJ system, notably in the context of respiratory diseases.^{58,59,82} Importantly, it was shown that the apelinergic system changes with age and that its restoration (by means of apelin treatment) reinforces circadian patterns and increases the mammalian healthspan.⁶⁰ The role of the apelinergic system in infection has not yet been established. Our data show that pharmacological activation of APJ signaling upregulates pulmonary anti-bacterial defenses. It remains to be seen whether APJ signaling, which is relevant in macrophage functions,⁶⁴ acted in our study as a macrophage-intrinsic circadian regulator of phagocytosis and bacterial killing. It is noteworthy that in young-adult mice, APJ was in part involved in the protection against pneumococcal infection triggered by SR8278.

Recent evidence indicates that the age-related misalignment of circadian rhythms can be corrected pharmacologically, for example by stimulating molecular oscillators.^{83,84} Pharmacological treatments based on the circadian clock include melatonin and agonists of the main components of the stabilizing loop (namely Rev-erbs and RORs), such as nobiletin.^{83,84} Treatment of respiratory infections in older adults by targeting the circadian system has not yet been investigated. Importantly, our present results showed that local administration of the Rev-erb- α antagonist SR8278 lowered the bacterial load in elderly mice. These findings are in line with those from Kirchner and colleagues, who recently used SR8278 as a circadian-enhancing agent to reduce infection of herpes simplex virus 1 in aging skins.⁸⁵ Altogether, these results highlighted the potential therapeutic utility of modulating the clock protein machinery to reduce the likelihood of infection in the aged population. It is noteworthy that the combination of apelin with SR8278 did not strengthen the latter's protective effect. This might be due to the low level of APJ expression in lungs from elderly mice and to SR8278's inability to enhance that expression.

Limitations of the study

Although our results provide insights into therapies that target the circadian system and might improve lung defenses in older individuals, data obtained in mice should be interpreted with caution. Indeed, this model does not reproduce all the characteristics of the circadian shift associated with age. Furthermore, mice (unlike humans) are nocturnal. It is noteworthy that our work was done exclusively in male mice, and there are known sex differences in pneumococcal infection in both humans and mice.⁸⁶ Another

limitation relates to our focus on AMs. Although our results are very much in line with a previous study in which aged macrophages were identified as potential targets of clock-based therapeutics for the control of lung infections,³⁸ other cell types might also be affected by age-mediated circadian irregularities. For example, epithelial cells have a strong intrinsic circadian cycle, and the latter can be impaired by stress; this might influence the outcome of lung infections.^{11,87} Although technically challenging,⁸⁸ the engraftment of young AMs (Rev-erb- α competent or deficient) into old mice would be helpful to firmly demonstrate the key role of AMs in altered immune defense in the elderly. Regarding the importance of the AM-neutrophil axis in anti-pneumococcal immune defense, altered rhythmicity of neutrophils might also be important. Lastly, it remains to be seen whether the treatment of elderly mice with SR8278 restores (at least in part) oscillations in pulmonary defenses. In conclusion, our study revealed a novel pathway involved in respiratory bacterial (at least pneumococcal) infections in elderly mice and provides new insights into the role of Rev-erb- α in pulmonary defenses. Our results suggest that age-related circadian impairments could be targeted in respiratory infectious disorders.

RESOURCE AVAILABILITY

Lead contact

Further information and requests for resources and reagents should be directed to and will be fulfilled by the lead contact, Dr. François Trottein (francois.trottein@pasteur-lille.fr).

Materials availability

This study did not generate new unique reagents.

Data and code availability

- Transcriptomic data of this study have been deposited in NCBI's Gene Expression Omnibus (GEO) and are publicly available. The accession numbers are listed in the [key resources table](#).
- This paper does not report original code.
- Crude data have been deposited at <https://doi.org/10.57745/ND3M71>. Any additional information required to reanalyze the data reported in this paper is available from the [lead contact](#) upon request.

ACKNOWLEDGMENTS

Support was provided in part by grants from the Agence Nationale de la Recherche: ANR-19-CE15-0033-01, DREAM (S.A., H.D., and F.T.), ANR-23-CE15-0014-01, GUTSY (F.T.), and ANR-Labex-EGID (EGID, ANR-10-LABX-46) (B.S., H.D., and B.P.). This project was also co-founded by the European Union under the European Region Development Fund and by Hauts de France Region Council (contract_20000007 and contract_20002842), the MEL (contract-2020-ESR-02 and contract-2020-ESR-06), and the French state (contract no. 2019/2020-R3-CTRL_IPL_Phase 3/4) (H.D. and F.T.). We thank the Fondation médicale pour la recherche (EQU202003010310) (H.D.).

AUTHOR CONTRIBUTIONS

H.D., B.P., and F.T. conceived and supervised the study. F.S.A., C.V.J., B.S., P.V., S.A., J.-C.S., H.D., B.P., and F.T. designed the experiments. F.S.A., C.V.J., and L. Delval performed the animal experiments and flow cytometry. M.B., L. Deruyter, and B.P. prepared and analyzed the RNAs for transcriptomic analyses. M.F., J.T.H., J.V., and B.P. performed analysis of the transcriptomic data. T.B. and R.G. prepared and analyzed the nanoparticles. F.S.A., C.V.J., and A.M. performed flow-cytometry experiments. P.B.R., V.S., and M.G.M. performed the phagocytosis and killing assays. L. Deruyter and S.H.

performed the RT-PCR. S.D. and S.S.-D. performed confocal analysis. F.S.A. performed the western blotting. M.B. and B.P. performed the ChIP experiment. F.S.A., C.V.J., P.B.R., P.V., M.F., H.D., B.P., and F.T. analyzed the data. F.S.A., B.P., and F.T. designed the figures. B.P. and F.T. drafted the manuscript. All authors revised the manuscript and provided critical comments. H.D., B.P., and F.T. obtained funding.

DECLARATION OF INTERESTS

H.D., B.P., and F.T. disclose a patent application related to the Rev-Erb antagonists for the treatment of lung infections.

STAR METHODS

Detailed methods are provided in the online version of this paper and include the following:

- KEY RESOURCES TABLE
- EXPERIMENTAL MODEL AND STUDY PARTICIPANT DETAILS
 - Mice and ethics statement
 - Bacteria
 - Cell line
- METHOD DETAILS
 - Diets
 - Infections and assessment of bacterial loads
 - Stimulation of pulmonary mononuclear cells and ELISA
 - Rev-erb agonist/antagonist treatment, depletion of alveolar macrophages, and apelin treatment
 - SR8278 incorporation into nanoparticles
 - RNA extraction, RNA sequencing analysis and statistical analysis
 - Microarray analysis and statistical analysis
 - Assessment of gene expression by quantitative RT-PCR
 - Chromatin immunoprecipitation assay
 - Flow cytometry
 - *In vitro* phagocytosis, ROS production and killing assay (MPI cells)
 - Collection of alveolar macrophages and phagocytosis assay
 - Generation of bone marrow-derived macrophages (BMDMs) and phagocytosis assay
 - Analysis of circadian phagocytosis (BMDMs)
 - Western blotting
- QUANTIFICATION AND STATISTICAL ANALYSIS

SUPPLEMENTAL INFORMATION

Supplemental information can be found online at <https://doi.org/10.1016/j.celrep.2025.115273>.

Received: May 16, 2024

Revised: October 8, 2024

Accepted: January 15, 2025

Published: February 4, 2025

REFERENCES

1. van der Poll, T., and Opal, S.M. (2009). Pathogenesis, treatment, and prevention of pneumococcal pneumonia. *Lancet Lond. Engl.* 374, 1543–1556. [https://doi.org/10.1016/S0140-6736\(09\)61114-4](https://doi.org/10.1016/S0140-6736(09)61114-4).
2. Shaw, A.C., Goldstein, D.R., and Montgomery, R.R. (2013). Age-dependent dysregulation of innate immunity. *Nat. Rev. Immunol.* 13, 875–887. <https://doi.org/10.1038/nri3547>.
3. Gonçalves, M.T., Mitchell, T.J., and Lord, J.M. (2016). Immune ageing and susceptibility to *Streptococcus pneumoniae*. *Biogerontology* 17, 449–465. <https://doi.org/10.1007/s10522-015-9614-8>.
4. Schneider, J.L., Rowe, J.H., Garcia-de-Alba, C., Kim, C.F., Sharpe, A.H., and Haigis, M.C. (2021). The aging lung: Physiology, disease, and immunity. *Cell* 184, 1990–2019. <https://doi.org/10.1016/j.cell.2021.03.005>.
5. Boe, D.M., Boule, L.A., and Kovacs, E.J. (2017). Innate immune responses in the ageing lung. *Clin. Exp. Immunol.* 187, 16–25. <https://doi.org/10.1111/cei.12881>.
6. Mohawk, J.A., Green, C.B., and Takahashi, J.S. (2012). Central and peripheral circadian clocks in mammals. *Annu. Rev. Neurosci.* 35, 445–462. <https://doi.org/10.1146/annurev-neuro-060909-153128>.
7. Albrecht, U. (2012). Timing to perfection: the biology of central and peripheral circadian clocks. *Neuron* 74, 246–260. <https://doi.org/10.1016/j.neuron.2012.04.006>.
8. Scheiermann, C., Gibbs, J., Ince, L., and Loudon, A. (2018). Clocking in to immunity. *Nat. Rev. Immunol.* 18, 423–437. <https://doi.org/10.1038/s41577-018-0008-4>.
9. Rijo-Ferreira, F., and Takahashi, J.S. (2019). Genomics of circadian rhythms in health and disease. *Genome Med.* 11, 82. <https://doi.org/10.1186/s13073-019-0704-0>.
10. Pourcet, B., and Duez, H. (2021). Nuclear Receptors and Clock Components in Cardiovascular Diseases. *Int. J. Mol. Sci.* 22, 9721. <https://doi.org/10.3390/ijms22189721>.
11. Gibbs, J., Ince, L., Matthews, L., Mei, J., Bell, T., Yang, N., Saer, B., Begley, N., Poolman, T., Pariollaud, M., et al. (2014). An epithelial circadian clock controls pulmonary inflammation and glucocorticoid action. *Nat. Med.* 20, 919–926. <https://doi.org/10.1038/nm.3599>.
12. Pariollaud, M., Gibbs, J.E., Hopwood, T.W., Brown, S., Begley, N., Vonslow, R., Poolman, T., Guo, B., Saer, B., Jones, D.H., et al. (2018). Circadian clock component REV-ERB α controls homeostatic regulation of pulmonary inflammation. *J. Clin. Invest.* 128, 2281–2296. <https://doi.org/10.1172/JCI93910>.
13. Mure, L.S., Le, H.D., Benegiamo, G., Chang, M.W., Rios, L., Jillani, N., Ngotto, M., Kariuki, T., Dkhissi-Benyahya, O., Cooper, H.M., and Panda, S. (2018). Diurnal transcriptome atlas of a primate across major neural and peripheral tissues. *Science* 359, eaao0318. <https://doi.org/10.1126/science.aao0318>.
14. Gibbs, J.E., Blaikley, J., Beesley, S., Matthews, L., Simpson, K.D., Boyce, S.H., Farrow, S.N., Else, K.J., Singh, D., Ray, D.W., and Loudon, A.S.I. (2012). The nuclear receptor REV-ERB α mediates circadian regulation of innate immunity through selective regulation of inflammatory cytokines. *Proc. Natl. Acad. Sci. USA* 109, 582–587. <https://doi.org/10.1073/pnas.1106750109>.
15. Preitner, N., Damiola, F., Lopez-Molina, L., Zakany, J., Duboule, D., Albrecht, U., and Schibler, U. (2002). The orphan nuclear receptor REV-ERB α controls circadian transcription within the positive limb of the mammalian circadian oscillator. *Cell* 110, 251–260. [https://doi.org/10.1016/s0092-8674\(02\)00825-5](https://doi.org/10.1016/s0092-8674(02)00825-5).
16. Yao, H., Sundar, I.K., Huang, Y., Gerloff, J., Sellix, M.T., Sime, P.J., and Rahman, I. (2015). Disruption of Sirtuin 1-Mediated Control of Circadian Molecular Clock and Inflammation in Chronic Obstructive Pulmonary Disease. *Am. J. Respir. Cell Mol. Biol.* 53, 782–792. <https://doi.org/10.1165/rcmb.2014-0474OC>.
17. Cho, H., Zhao, X., Hatori, M., Yu, R.T., Barish, G.D., Lam, M.T., Chong, L.-W., DiTacchio, L., Atkins, A.R., Glass, C.K., et al. (2012). Regulation of circadian behaviour and metabolism by REV-ERB α and REV-ERB β . *Nature* 485, 123–127. <https://doi.org/10.1038/nature11048>.
18. Kojetin, D.J., and Burris, T.P. (2014). REV-ERB and ROR nuclear receptors as drug targets. *Nat. Rev. Drug Discov.* 13, 197–216. <https://doi.org/10.1038/nrd4100>.
19. Sato, S., Sakurai, T., Ogasawara, J., Takahashi, M., Izawa, T., Imaizumi, K., Taniguchi, N., Ohno, H., and Kizaki, T. (2014). A circadian clock gene, Rev-erb α , modulates the inflammatory function of macrophages through the negative regulation of Ccl2 expression. *J. Immunol.* 1, 407–417. <https://doi.org/10.4049/jimmunol.1301982>.
20. Griffin, P., Dimitry, J.M., Sheehan, P.W., Lananna, B.V., Guo, C., Robinette, M.L., Hayes, M.E., Cedeño, M.R., Nadarajah, C.J., Ezerskiy, L.A., et al. (2019). Circadian clock protein Rev-erb α regulates

- neuroinflammation. *Proc. Natl. Acad. Sci. USA* 116, 5102–5107. <https://doi.org/10.1073/pnas.1812405116>.
21. Pourceret, B., Zecchin, M., Ferri, L., Beauchamp, J., Sitalua, S., Billon, C., Delhayé, S., Vanhoutte, J., Mayeuf-Louchart, A., Thorel, Q., et al. (2018). Nuclear Receptor Subfamily 1 Group D Member 1 Regulates Circadian Activity of NLRP3 Inflammasome to Reduce the Severity of Fulminant Hepatitis in Mice. *Gastroenterology* 154, 1449–1464.e20. <https://doi.org/10.1053/j.gastro.2017.12.019>.
 22. Ma, H., Zhong, W., Jiang, Y., Fontaine, C., Li, S., Fu, J., Olkkonen, V.M., Staels, B., and Yan, D. (2013). Increased atherosclerotic lesions in LDL receptor deficient mice with hematopoietic nuclear receptor Rev-erb α knock-down. *J. Am. Heart Assoc.* 2, e000235. <https://doi.org/10.1161/JAHA.113.000235>.
 23. Yu, X., Rollins, D., Ruhn, K.A., Stubblefield, J.J., Green, C.B., Kashiwada, M., Rothman, P.B., Takahashi, J.S., and Hooper, L.V. (2013). TH17 cell differentiation is regulated by the circadian clock. *Science* 342, 727–730. <https://doi.org/10.1126/science.1243884>.
 24. Curtis, A.M., Bellet, M.M., Sassone-Corsi, P., and O'Neill, L.A.J. (2014). Circadian clock proteins and immunity. *Immunity* 40, 178–186. <https://doi.org/10.1016/j.immuni.2014.02.002>.
 25. Tognini, P., Thaiss, C.A., Elinav, E., and Sassone-Corsi, P. (2017). Circadian Coordination of Antimicrobial Responses. *Cell Host Microbe* 22, 185–192. <https://doi.org/10.1016/j.chom.2017.07.007>.
 26. Feigin, R.D., San Joaquin, V.H., Haymond, M.W., and Wyatt, R.G. (1969). Daily periodicity of susceptibility of mice to pneumococcal infection. *Nature* 224, 379–380. <https://doi.org/10.1038/224379a0>.
 27. Hames, R.G., Jasuinaite, Z., Ercoli, G., Wanford, J.J., Carreno, D., Straatman, K., Martinez-Pomares, L., Yesilkaya, H., Glenn, S., Moxon, E.R., et al. (2022). Diurnal Differences in Intracellular Replication Within Splenic Macrophages Correlates With the Outcome of Pneumococcal Infection. *Front. Immunol.* 13, 907461. <https://doi.org/10.3389/fimmu.2022.907461>.
 28. Scheiermann, C., Kunisaki, Y., and Frenette, P.S. (2013). Circadian control of the immune system. *Nat. Rev. Immunol.* 13, 190–198. <https://doi.org/10.1038/nri3386>.
 29. Man, K., Loudon, A., and Chawla, A. (2016). Immunity around the clock. *Science* 354, 999–1003. <https://doi.org/10.1126/science.aah4966>.
 30. He, W., Holtkamp, S., Hergenhan, S.M., Kraus, K., de Juan, A., Weber, J., Bradfield, P., Grenier, J.M.P., Pelletier, J., Druzd, D., et al. (2018). Circadian Expression of Migratory Factors Establishes Lineage-Specific Signatures that Guide the Homing of Leukocyte Subsets to Tissues. *Immunity* 49, 1175–1190.e7. <https://doi.org/10.1016/j.immuni.2018.10.007>.
 31. Kitchen, G.B., Cunningham, P.S., Poolman, T.M., Iqbal, M., Maidstone, R., Baxter, M., Bagnall, J., Begley, N., Saer, B., Hussell, T., et al. (2020). The clock gene Bmal1 inhibits macrophage motility, phagocytosis, and impairs defense against pneumonia. *Proc. Natl. Acad. Sci. USA* 117, 1543–1551. <https://doi.org/10.1073/pnas.1915932117>.
 32. Wang, C., Lutes, L.K., Barnoud, C., and Scheiermann, C. (2022). The circadian immune system. *Sci. Immunol.* 7, eabm2465. <https://doi.org/10.1126/sciimmunol.abm2465>.
 33. López-Otín, C., Blasco, M.A., Partridge, L., Serrano, M., and Kroemer, G. (2013). The hallmarks of aging. *Cell* 153, 1194–1217. <https://doi.org/10.1016/j.cell.2013.05.039>.
 34. Sundar, I.K., Yao, H., Sellix, M.T., and Rahman, I. (2015). Circadian molecular clock in lung pathophysiology. *Am. J. Physiol. Lung Cell Mol. Physiol.* 309, L1056–L1075. <https://doi.org/10.1152/ajplung.00152.2015>.
 35. Bechtold, D.A., Gibbs, J.E., and Loudon, A.S.I. (2010). Circadian dysfunction in disease. *Trends Pharmacol. Sci.* 31, 191–198. <https://doi.org/10.1016/j.tips.2010.01.002>.
 36. Morris, C.J., Purvis, T.E., Hu, K., and Scheer, F.A.J.L. (2016). Circadian misalignment increases cardiovascular disease risk factors in humans. *Proc. Natl. Acad. Sci. USA* 113, E1402–E1411. <https://doi.org/10.1073/pnas.1516953113>.
 37. Kondratova, A.A., and Kondratov, R.V. (2012). The circadian clock and pathology of the ageing brain. *Nat. Rev. Neurosci.* 13, 325–335. <https://doi.org/10.1038/nrn3208>.
 38. Blacher, E., Tsai, C., Litichevskiy, L., Shipony, Z., Iweka, C.A., Schneider, K.M., Chuluun, B., Heller, H.C., Menon, V., Thaiss, C.A., and Andreasson, K.I. (2022). Aging disrupts circadian gene regulation and function in macrophages. *Nat. Immunol.* 23, 229–236. <https://doi.org/10.1038/s41590-021-01083-0>.
 39. Hayashi, M., Shimba, S., and Tezuka, M. (2007). Characterization of the molecular clock in mouse peritoneal macrophages. *Biol. Pharm. Bull.* 30, 621–626. <https://doi.org/10.1248/bpb.30.621>.
 40. Keller, M., Mazuch, J., Abraham, U., Eom, G.D., Herzog, E.D., Volk, H.-D., Kramer, A., and Maier, B. (2009). A circadian clock in macrophages controls inflammatory immune responses. *Proc. Natl. Acad. Sci. USA* 106, 21407–21412. <https://doi.org/10.1073/pnas.0906361106>.
 41. Oliva-Ramírez, J., Moreno-Altamirano, M.M.B., Pineda-Olvera, B., Cauich-Sánchez, P., and Sánchez-García, F.J. (2014). Crosstalk between circadian rhythmicity, mitochondrial dynamics and macrophage bactericidal activity. *Immunology* 143, 490–497. <https://doi.org/10.1111/imm.12329>.
 42. Chaguza, C., Yang, M., Jacques, L.C., Bentley, S.D., and Kadioglu, A. (2022). Serotype 1 pneumococcus: epidemiology, genomics, and disease mechanisms. *Trends Microbiol.* 30, 581–592. <https://doi.org/10.1016/j.tim.2021.11.007>.
 43. Dutta, S., and Sengupta, P. (2016). Men and mice: Relating their ages. *Life Sci.* 152, 244–248. <https://doi.org/10.1016/j.lfs.2015.10.025>.
 44. Gordon, S.B., Irving, G.R., Lawson, R.A., Lee, M.E., and Read, R.C. (2000). Intracellular trafficking and killing of *Streptococcus pneumoniae* by human alveolar macrophages are influenced by opsonins. *Infect. Immun.* 68, 2286–2293. <https://doi.org/10.1128/IAI.68.4.2286-2293.2000>.
 45. Yamada, M., Gomez, J.C., Chugh, P.E., Lowell, C.A., Dinauer, M.C., Dittmer, D.P., and Doerschuk, C.M. (2011). Interferon- γ production by neutrophils during bacterial pneumonia in mice. *Am. J. Respir. Crit. Care Med.* 183, 1391–1401. <https://doi.org/10.1164/rccm.201004-0592OC>.
 46. Ivanov, S., Paget, C., and Trottein, F. (2014). Role of non-conventional T lymphocytes in respiratory infections: the case of the pneumococcus. *PLoS Pathog.* 10, e1004300. <https://doi.org/10.1371/journal.ppat.1004300>.
 47. Hassane, M., Demon, D., Soulard, D., Fontaine, J., Keller, L.E., Patin, E.C., Porte, R., Prinz, I., Ryffel, B., Kadioglu, A., et al. (2017). Neutrophilic NLRP3 inflammasome-dependent IL-1 β secretion regulates the $\gamma\delta$ T1 cell response in respiratory bacterial infections. *Mucosal Immunol.* 10, 1056–1068. <https://doi.org/10.1038/mi.2016.113>.
 48. Thaben, P.F., and Westermark, P.O. (2014). Detecting rhythms in time series with RAIN. *J. Biol. Rhythms* 29, 391–400. <https://doi.org/10.1177/0748730414553029>.
 49. Cain, D.W., and Cidlowski, J.A. (2017). Immune regulation by glucocorticoids. *Nat. Rev. Immunol.* 17, 233–247. <https://doi.org/10.1038/nri.2017.1>.
 50. Vandel, J., Gheeraert, C., Staels, B., Eeckhoute, J., Lefebvre, P., and Du-bois-Chevalier, J. (2020). GIANT: galaxy-based tool for interactive analysis of transcriptomic data. *Sci. Rep.* 10, 19835. <https://doi.org/10.1038/s41598-020-76769-w>.
 51. Duez, H., and Staels, B. (2008). Rev-erb alpha gives a time cue to metabolism. *FEBS Lett.* 582, 19–25. <https://doi.org/10.1016/j.febslet.2007.08.032>.
 52. Vieira, E., Marroquín, L., Figueroa, A.L.C., Merino, B., Fernandez-Ruiz, R., Nadal, A., Burris, T.P., Gomis, R., and Quesada, I. (2013). Involvement of the clock gene Rev-erb alpha in the regulation of glucagon secretion in pancreatic alpha-cells. *PLoS One* 8, e69939. <https://doi.org/10.1371/journal.pone.0069939>.

53. Kojetin, D., Wang, Y., Kamenecka, T.M., and Burris, T.P. (2011). Identification of SR8278, a synthetic antagonist of the nuclear heme receptor REV-ERB. *ACS Chem. Biol.* 6, 131–134. <https://doi.org/10.1021/cb1002575>.
54. Mass, E. (2023). The stunning clodronate. *J. Exp. Med.* 220, e20230339. <https://doi.org/10.1084/jem.20230339>.
55. Fejer, G., Wegner, M.D., Györy, I., Cohen, I., Engelhard, P., Voronov, E., Manke, T., Ruzsics, Z., Dölken, L., Prazeres da Costa, O., et al. (2013). Nontransformed, GM-CSF-dependent macrophage lines are a unique model to study tissue macrophage functions. *Proc. Natl. Acad. Sci. USA* 110, E2191–E2198. <https://doi.org/10.1073/pnas.1302877110>.
56. Woo, M., Wood, C., Kwon, D., Park, K.H.P., Fejer, G., and Delorme, V. (2018). Mycobacterium tuberculosis Infection and Innate Responses in a New Model of Lung Alveolar Macrophages. *Front. Immunol.* 9, 438. <https://doi.org/10.3389/fimmu.2018.00438>.
57. West, A.P., Brodsky, I.E., Rahner, C., Woo, D.K., Erdjument-Bromage, H., Tempst, P., Walsh, M.C., Choi, Y., Shadel, G.S., and Ghosh, S. (2011). TLR signalling augments macrophage bactericidal activity through mitochondrial ROS. *Nature* 472, 476–480. <https://doi.org/10.1038/nature09973>.
58. Castan-Laurell, I., Masri, B., and Valet, P. (2019). The apelin/APJ system as a therapeutic target in metabolic diseases. *Expert Opin. Ther. Targets* 23, 215–225. <https://doi.org/10.1080/14728222.2019.1561871>.
59. Yan, J., Wang, A., Cao, J., and Chen, L. (2020). Apelin/APJ system: an emerging therapeutic target for respiratory diseases. *Cell. Mol. Life Sci.* 77, 2919–2930. <https://doi.org/10.1007/s0018-020-03461-7>.
60. Rai, R., Ghosh, A.K., Eren, M., Mackie, A.R., Levine, D.C., Kim, S.-Y., Cerdnaes, J., Ramirez, V., Procissi, D., Smith, L.H., et al. (2017). Downregulation of the Apelinergic Axis Accelerates Aging, whereas Its Systemic Restoration Improves the Mammalian Healthspan. *Cell Rep.* 21, 1471–1480. <https://doi.org/10.1016/j.celrep.2017.10.057>.
61. Vinel, C., Lukjanenko, L., Batut, A., Deleruyelle, S., Pradère, J.-P., Le Goñidec, S., Dortignac, A., Geoffre, N., Pereira, O., Karaz, S., et al. (2018). The exerkine apelin reverses age-associated sarcopenia. *Nat. Med.* 24, 1360–1371. <https://doi.org/10.1038/s41591-018-0131-6>.
62. Kinjo, T., Higashi, H., Uno, K., and Kuramoto, N. (2021). Apelin/Apelin Receptor System: Molecular Characteristics, Physiological Roles, and Prospects as a Target for Disease Prevention and Pharmacotherapy. *Curr. Mol. Pharmacol.* 14, 210–219. <https://doi.org/10.2174/1874467213666200602133032>.
63. Murza, A., Belleville, K., Longpré, J.-M., Sarret, P., and Marsault, É. (2014). Stability and degradation patterns of chemically modified analogs of apelin-13 in plasma and cerebrospinal fluid. *Biopolymers* 102, 297–303. <https://doi.org/10.1002/bip.22498>.
64. Arababadi, M.K., Asadikaram, P., and Asadikaram, G. (2019). APLN/APJ pathway: The key regulator of macrophage functions. *Life Sci.* 232, 116645. <https://doi.org/10.1016/j.lfs.2019.116645>.
65. Williams, A.E., José, R.J., Brown, J.S., and Chambers, R.C. (2015). Enhanced inflammation in aged mice following infection with *Streptococcus pneumoniae* is associated with decreased IL-10 and augmented chemokine production. *Am. J. Physiol. Lung Cell Mol. Physiol.* 308, L539–L549. <https://doi.org/10.1152/ajplung.00141.2014>.
66. McMahan, R.H., Hulsebus, H.J., Najarro, K.M., Giesy, L.E., Frank, D.N., Orlicky, D.J., and Kovacs, E.J. (2022). Age-Related Intestinal Dysbiosis and Enrichment of Gut-specific Bacteria in the Lung Are Associated With Increased Susceptibility to *Streptococcus pneumoniae* Infection in Mice. *Front. Aging* 3, 859991. <https://doi.org/10.3389/fragi.2022.859991>.
67. Menter, T., Giebing-Kroell, C., Grubeck-Loebenstein, B., and Tzankov, A. (2014). Characterization of the inflammatory infiltrate in *Streptococcus pneumoniae* pneumonia in young and elderly patients. *Pathobiology* 81, 160–167. <https://doi.org/10.1159/000360165>.
68. Inokawa, H., Umemura, Y., Shimba, A., Kawakami, E., Koike, N., Tsuchiya, Y., Ohashi, M., Minami, Y., Cui, G., Asahi, T., et al. (2020). Chronic circadian misalignment accelerates immune senescence and abbreviates lifespan in mice. *Sci. Rep.* 10, 2569. <https://doi.org/10.1038/s41598-020-59541-y>.
69. Fonken, L.K., Kitt, M.M., Gaudet, A.D., Barrientos, R.M., Watkins, L.R., and Maier, S.F. (2016). Diminished circadian rhythms in hippocampal microglia may contribute to age-related neuroinflammatory sensitization. *Neurobiol. Aging* 47, 102–112. <https://doi.org/10.1016/j.neurobiolaging.2016.07.019>.
70. Sato, S., Solanas, G., Peixoto, F.O., Bee, L., Symeonidi, A., Schmidt, M.S., Brenner, C., Masri, S., Benitah, S.A., and Sassone-Corsi, P. (2017). Circadian Reprogramming in the Liver Identifies Metabolic Pathways of Aging. *Cell* 170, 664–677.e11. <https://doi.org/10.1016/j.cell.2017.07.042>.
71. Solanas, G., Peixoto, F.O., Perdigero, E., Jardí, M., Ruiz-Bonilla, V., Datta, D., Symeonidi, A., Castellanos, A., Welz, P.-S., Caballero, J.M., et al. (2017). Aged Stem Cells Reprogram Their Daily Rhythmic Functions to Adapt to Stress. *Cell* 170, 678–692.e20. <https://doi.org/10.1016/j.cell.2017.07.035>.
72. Wolff, C.A., Gutierrez-Monreal, M.A., Meng, L., Zhang, X., Douma, L.G., Costello, H.M., Douglas, C.M., Ebrahimi, E., Pham, A., Oliveira, A.C., et al. (2023). Defining the age-dependent and tissue-specific circadian transcriptome in male mice. *Cell Rep.* 42, 111982. <https://doi.org/10.1016/j.celrep.2022.111982>.
73. Jiang, H., Ye, X.-P., Yang, Z.-Y., Zhan, M., Wang, H.-N., Cao, H.-M., Xie, H.-J., Pan, C.-M., Song, H.-D., and Zhao, S.-X. (2013). Aldosterone directly affects apelin expression and secretion in adipocytes. *J. Mol. Endocrinol.* 51, 37–48. <https://doi.org/10.1530/JME-13-0025>.
74. Lv, S.-Y., Yang, Y.-J., and Chen, Q. (2013). Regulation of feeding behavior, gastrointestinal function and fluid homeostasis by apelin. *Peptides* 44, 87–92. <https://doi.org/10.1016/j.peptides.2013.03.024>.
75. Torra, I.P., Tsibulsky, V., Delaunay, F., Saladin, R., Laudet, V., Fruchart, J.C., Kosykh, V., and Staels, B. (2000). Circadian and glucocorticoid regulation of Rev-erbalpha expression in liver. *Endocrinology* 141, 3799–3806. <https://doi.org/10.1210/endo.141.10.7708>.
76. Caratti, G., Iqbal, M., Hunter, L., Kim, D., Wang, P., Vonslow, R.M., Begley, N., Tetley, A.J., Woodburn, J.L., Pariollaud, M., et al. (2018). RE-VERBa couples the circadian clock to hepatic glucocorticoid action. *J. Clin. Invest.* 128, 4454–4471. <https://doi.org/10.1172/JCI96138>.
77. Murayama, Y., Yahagi, N., Takeuchi, Y., Aita, Y., Mehrasad Saber, Z., Wada, N., Li, E., Piao, X., Sawada, Y., Shikama, A., et al. (2019). Glucocorticoid receptor suppresses gene expression of Rev-erbα (Nr1d1) through interaction with the CLOCK complex. *FEBS Lett.* 593, 423–432. <https://doi.org/10.1002/1873-3468.13328>.
78. Wang, Q., Sundar, I.K., Lucas, J.H., Park, J.-G., Nogales, A., Martinez-Sobrido, L., and Rahman, I. (2023). Circadian clock molecule REV-erbα regulates lung fibrotic progression through collagen stabilization. *Nat. Commun.* 14, 1295. <https://doi.org/10.1038/s41467-023-36896-0>.
79. Griepentrog, J.E., Zhang, X., Lewis, A.J., Gianfrate, G., Labiner, H.E., Zou, B., Xiong, Z., Lee, J.S., and Rosengart, M.R. (2020). Frontline Science: Rev-Erbα links blue light with enhanced bacterial clearance and improved survival in murine *Klebsiella pneumoniae* pneumonia. *J. Leukoc. Biol.* 107, 11–25. <https://doi.org/10.1002/JLB.4H10519-155R>.
80. Lee, J., Kim, D.E., Griffin, P., Sheehan, P.W., Kim, D.-H., Musiek, E.S., and Yoon, S.-Y. (2020). Inhibition of REV-ERBs stimulates microglial amyloid-beta clearance and reduces amyloid plaque deposition in the 5XFAD mouse model of Alzheimer's disease. *Aging Cell* 19, e13078. <https://doi.org/10.1111/acel.13078>.
81. Jang, D.-Y., Yang, B., You, M.-J., Rim, C., Kim, H.-J., Sung, S., and Kwon, M.-S. (2023). Fluoxetine Decreases Phagocytic Function via REV-ERBα in Microglia. *Neurochem. Res.* 48, 196–209. <https://doi.org/10.1007/s11064-022-03733-7>.

82. Shin, K., Kenward, C., and Rainey, J.K. (2017). Apelinergic System Structure and Function. *Compr. Physiol.* 8, 407–450. <https://doi.org/10.1002/cphy.c170028>.
83. Kim, E., Yoo, S.-H., and Chen, Z. (2022). Circadian stabilization loop: the regulatory hub and therapeutic target promoting circadian resilience and physiological health. *F1000Res.* 11, 1236. <https://doi.org/10.12688/f1000research.126364.2>.
84. Rawashdeh, O., and Maronde, E. (2012). The hormonal Zeitgeber melatonin: role as a circadian modulator in memory processing. *Front. Mol. Neurosci.* 5, 27. <https://doi.org/10.3389/fnmol.2012.00027>.
85. Kirchner, S.J., Lei, V., Kim, P.T., Patel, M., Shannon, J.L., Corcoran, D., Hughes, D., Waters, D.K., Dzirasa, K., Erdmann, D., et al. (2023). An aging-susceptible circadian rhythm controls cutaneous antiviral immunity. *JCI Insight* 8, e171548. <https://doi.org/10.1172/jci.insight.171548>.
86. Kadioglu, A., Cuppone, A.M., Trappetti, C., List, T., Spreafico, A., Pozzi, G., Andrew, P.W., and Oggioni, M.R. (2011). Sex-based differences in susceptibility to respiratory and systemic pneumococcal disease in mice. *J. Infect. Dis.* 204, 1971–1979. <https://doi.org/10.1093/infdis/jir657>.
87. Issah, Y., Naik, A., Tang, S.Y., Forrest, K., Brooks, T.G., Lahens, N., Theken, K.N., Mermigas, M., Sehgal, A., Worthen, G.S., et al. (2021). Loss of circadian protection against influenza infection in adult mice exposed to hyperoxia as neonates. *Elife* 10, e61241. <https://doi.org/10.7554/elife.61241>.
88. McQuattie-Pimentel, A.C., Ren, Z., Joshi, N., Watanabe, S., Stoeger, T., Chi, M., Lu, Z., Sichizya, L., Aillon, R.P., Chen, C.-I., et al. (2021). The lung microenvironment shapes a dysfunctional response of alveolar macrophages in aging. *J. Clin. Invest.* 131, e140299. <https://doi.org/10.1172/JCI140299>.
89. Barthelemy, A., Ivanov, S., Fontaine, J., Soulard, D., Bouabe, H., Paget, C., Faveeuw, C., and Trottein, F. (2017). Influenza A virus-induced release of interleukin-10 inhibits the anti-microbial activities of invariant natural killer T cells during invasive pneumococcal superinfection. *Mucosal Immunol.* 10, 460–469. <https://doi.org/10.1038/mi.2016.49>.
90. Ishida, J., Hashimoto, T., Hashimoto, Y., Nishiwaki, S., Iguchi, T., Harada, S., Sugaya, T., Matsuzaki, H., Yamamoto, R., Shiota, N., et al. (2004). Regulatory roles for APJ, a seven-transmembrane receptor related to angiotensin-type 1 receptor in blood pressure in vivo. *J Biol Chem* 279, 26274–26279. <https://doi.org/10.1074/jbc.M404149200>.
91. Carlucci, M., Kriščiūnas, A., Li, H., Gibas, P., Koncevičius, K., Petronis, A., and Oh, G. (2019). DiscoRhythm: an easy-to-use web application and R package for discovering rhythmicity. *Bioinforma. Oxf. Engl.* 36, 1952–1954. <https://doi.org/10.1093/bioinformatics/btz834>.
92. Kleverov, M., Zenkova, D., Kamenev, V., Sablina, M., Artyomov, M.N., and Sergushichev, A.A. (2024). Phantasis, a web application for visual and interactive gene expression analysis. *Elife* 13, e85722. <https://doi.org/10.7554/elife.85722>.
93. Bourguignon, T., Torrano, A.A., Houel-Renault, L., Machelart, A., Brodin, P., and Gref, R. (2021). An original methodology to study polymeric nanoparticle-macrophage interactions: Nanoparticle tracking analysis in cell culture media and quantification of the internalized objects. *Int. J. Pharm.* 610, 121202. <https://doi.org/10.1016/j.ijpharm.2021.121202>.
94. Kopylova, E., Noé, L., and Touzet, H. (2012). SortMeRNA: fast and accurate filtering of ribosomal RNAs in metatranscriptomic data. *Bioinforma. Oxf. Engl.* 28, 3211–3217. <https://doi.org/10.1093/bioinformatics/bts611>.
95. Dobin, A., Davis, C.A., Schlesinger, F., Drenkow, J., Zaleski, C., Jha, S., Batut, P., Chaisson, M., and Gingeras, T.R. (2013). STAR: ultrafast universal RNA-seq aligner. *Bioinforma. Oxf. Engl.* 29, 15–21. <https://doi.org/10.1093/bioinformatics/bts635>.
96. Patro, R., Duggal, G., Love, M.I., Irizarry, R.A., and Kingsford, C. (2017). Salmon provides fast and bias-aware quantification of transcript expression. *Nat. Methods* 14, 417–419. <https://doi.org/10.1038/nmeth.4197>.
97. Love, M.I., Huber, W., and Anders, S. (2014). Moderated estimation of fold change and dispersion for RNA-seq data with DESeq2. *Genome Biol.* 15, 550. <https://doi.org/10.1186/s13059-014-0550-8>.
98. Wu, T., Hu, E., Xu, S., Chen, M., Guo, P., Dai, Z., Feng, T., Zhou, L., Tang, W., Zhan, L., et al. (2021). clusterProfiler 4.0: A universal enrichment tool for interpreting omics data. *Innovation* 2, 100141. <https://doi.org/10.1016/j.xinn.2021.100141>.
99. Afgan, E., Baker, D., Batut, B., van den Beek, M., Bouvier, D., Cech, M., Chilton, J., Clements, D., Coraor, N., Grüning, B.A., et al. (2018). The Galaxy platform for accessible, reproducible and collaborative biomedical analyses: 2018 update. *Nucleic Acids Res.* 46, W537–W544. <https://doi.org/10.1093/nar/gky379>.
100. Ritchie, M.E., Phipson, B., Wu, D., Hu, Y., Law, C.W., Shi, W., and Smyth, G.K. (2015). limma powers differential expression analyses for RNA-sequencing and microarray studies. *Nucleic Acids Res.* 43, e47. <https://doi.org/10.1093/nar/gkv007>.
101. Machado, M.G., Patente, T.A., Rouillé, Y., Heumel, S., Melo, E.M., Deruyter, L., Pourcet, B., Sencio, V., Teixeira, M.M., and Trottein, F. (2022). Acetate Improves the Killing of *Streptococcus pneumoniae* by Alveolar Macrophages via NLRP3 Inflammasome and Glycolysis-HIF-1 α Axis. *Front. Immunol.* 13, 773261. <https://doi.org/10.3389/fimmu.2022.773261>.

STAR★METHODS
KEY RESOURCES TABLE

REAGENT or RESOURCE	SOURCE	IDENTIFIER
Antibodies		
Rat monoclonal anti-mouse CD45 (BV510)	BioLegend	Cat# 103138, clone 30-F11, RRID: AB_2563061
Rat monoclonal anti-mouse CD45 (AF700)	BioLegend	Cat# #103128, clone 30-FII, RRID: AB_493715
Rat monoclonal anti-mouse CD45 (BV605)	BioLegend	Cat# #103140, clone 30-FII, RRID: AB_2562342
Rat monoclonal anti-mouse CD19 (FITC)	BioLegend	Cat# 115506, clone 6D5, RRID: AB_313641
Rat monoclonal anti-mouse CD3 (APCCy7)	BioLegend	Cat #100222, clone 17A2, RRID: AB_2242784
Rat monoclonal anti-mouse CD4 (APCCy7)	BioLegend	Cat# #100414, clone GK1.5, RRID: AB_312699
Rat monoclonal anti-mouse CD8 α (FITC)	BioLegend	Cat# #100706, clone 53-6.7, RRID: AB_312745
Hamster monoclonal anti-mouse TCRgd (PerCpCy5.5)	BioLegend	Cat# #118118, clone GL3, RRID: AB_10612756
Hamster monoclonal anti-mouse TCRb (PE/Cy7)	BioLegend	Cat# 109222, clone H57-597, RRID: AB_893625
Mouse monoclonal anti-mouse NK1.1 (PE)	BioLegend	Cat# 156504, clone S17016D, RRID: AB_2783136
Rat monoclonal anti-mouse CD11b (PerCP/Cy5.5)	BioLegend	Cat# 101228, clone M1/70, RRID: AB_893232
Rat monoclonal anti-mouse CD11b (AF700)	BioLegend	Cat# 101222, clone M1/70, RRID: AB_493705
Hamster monoclonal anti-mouse CD11c (PECy7)	BioLegend	Cat# #117318, clone N418, RRID: AB_313775
Rat monoclonal anti-mouse Ly6G (APCCy7)	BioLegend	Cat# #127624, clone 1A8, RRID: AB_10640819
Rat monoclonal anti-mouse CD64 (APC)	BioLegend	Cat# 161006, clone S18017D, RRID: AB_2910336
Mouse monoclonal anti-mouse F4/80 (FITC)	BioLegend	Cat #157310, clone QA17A29, RRID: AB_2876535
Rat monoclonal anti-mouse MHCII (AF700)	BioLegend	Cat# 107622, clone M5/114.15.2, RRID: AB_493727
Rat monoclonal anti-mouse CD103 (FITC)	BioLegend	Cat# #110908, clone W19396D, RRID: AB_2936716
Rat monoclonal anti-mouse Ly6C (AF700)	BioLegend	Cat #128024, clone HK 1.4, RRID: AB_10643270
Rat monoclonal anti-mouse IL-17A (PE)	BioLegend	Cat #506904, clone TC11-18H10.1 RRID: AB_315464
Rat monoclonal anti-mouse CD206 (MMR, mannose receptor) (PE/Cyanine5)	BioLegend	Cat #141740, clone C068C2 RRID: AB_2910297
Rat monoclonal anti-mouse CD204 (Msrl, macrophage scavenger receptor 1) (APC)	BioLegend	Cat #154712, clone 1F8C33 RRID: AB_2892311
Hamster monoclonal anti-mouse CD36 (APC/Fire™ 750)	BioLegend	Cat #102618, clone HM36 RRID: AB_2750186

(Continued on next page)

Continued

REAGENT or RESOURCE	SOURCE	IDENTIFIER
Rat monoclonal anti-mouse Siglec F (PE)	BD Biosciences	Cat #562068, E50-2440, RRID: AB_394341
Rat monoclonal anti-mouse Siglec F (BV421)	BD Biosciences	Cat #562681, clone LOU/C, RRID: AB_2722581
Hamster monoclonal anti-mouse CD11c (FITC)	BD Biosciences	Cat #557400, clone HL3 RRID: AB_396683
Rat monoclonal anti-mouse F4/80 (APC)	BD Biosciences	Cat #566787, clone BM8, RRID: AB_2869866
Rat monoclonal anti-mouse -IFN γ (APC)	BD Biosciences	Cat #554413, clone XMG1.2 RRID: AB_398551
Rat recombinant anti-mouse IL-17A (PE)	BD Biosciences	Cat #559502, clone TC11-18H10 RRID: AB_397256
Rabbit recombinant multiclonal to APJ Receptor	Abcam	Cat # ab308018, clone: RP23040146
Mouse monoclonal anti mouse β -actin	Sigma Aldrich	Cat # A5441, clone AC-15 RRID: AB_47644
Goat anti-rabbit (IgG) secondary antibody (HRP)	Abcam	Cat # ab6721, RRID: AB_955447
Rabbit monoclonal anti-mouse Rev-erb- α	Cell Signaling Technology	Cat #13418, clone E1Y6D RRID: AB_2630359
Mouse monoclonal anti- H3K27me3	Abcam	Cat # ab6002, clone 3002 RRID: AB_305237
Bacterial and virus strains		
<i>Streptococcus pneumoniae</i> (clinical isolate E1586)	Barthelemy et al. ⁸⁹	N/A
Chemicals and antibiotics		
SR9009	Tocris Bioscience	Cat# 5855, RRID: N/A
SR8278	Tocris Bioscience	Cat# 4463, RRID: N/A
[Pyr1]-Apelin-13	Sigma Aldrich	Cat# 217082-60-5, RRID: N/A
Propidium iodide	BioLegend	Cat# 421301, RRID: N/A
Power SYBR TM Green PCR Master Mix	ThermoFisher Scientific	Cat# 4367660, RRID: N/A
CellMask TM Green Plasma Membrane Stain	ThermoFisher Scientific	Cat# C37608, RRID: N/A
DAPI	ThermoFisher Scientific	Cat# D1306, RRID: N/A
Clodronate liposome	Liposoma	Cat# CP-005-005, RRID: N/A
Penicillin	Sigma-Aldrich	Cat# N13752, RRID: N/A
Streptomycin	Sigma-Aldrich	Cat# S9137, RRID: N/A
Critical commercial assays		
High-Capacity RNA-to-cDNA TM Kit	ThermoFisher Scientific	Cat# 4387406, RRID: N/A
NucleoSpin [®] RNA	Macherey-Nagel	Cat# 740955, RRID: N/A
CellROX [®] Oxidative Stress Reagents	Life technologies, #C10422)	Cat#C10422, RRID: N/A
Deposited data		
RNA-seq	This paper	GEO: 261207 and 261234
Experimental models: Cell line		
MPI	Kojetin et al. ⁵³	N/A
Experimental models: Organisms/strains		
C57BL/6 mice	Janvier Labs, France	SC-C57J-M
<i>Nr1d1</i> ^{-/-} mice	Pourcet et al. ²¹	N/A
<i>Apj</i> ^{-/-} mice	Ishida et al. ⁹⁰	N/A

(Continued on next page)

Continued

REAGENT or RESOURCE	SOURCE	IDENTIFIER
Oligonucleotides		
<i>Gapdh</i>	Forward 5'-GCAAAGTGGAGATTGTTGCCA-3' Reverse 5'-GCCTGACTGTGCCGTTGA-3'	
<i>Nr1d1</i>	Forward 5'-TGGCCTCAGGCTTCACTATG-3' Reverse 5'-CCGTTGCTTCTCTCTTGGG-3'	
<i>Arntl</i>	Forward 5'-GGACTTCGCCTCACCTGTC-3' Reverse 5'-ACCGTATTTCCCCGTC-3'	
<i>Apj</i>	Forward 5'-TCGGCTAAGGCTCGAGTC-3' Reverse 5'-CGTCTGTGGAACGGAACAC-3'	
<i>Ccl2</i>	Forward 5'- GCAGCAGGTGTCCAAAGAA-3' Reverse 5'- TCATTTGGTTCGATCCAGGT-3'	
<i>Cxcl1</i>	Forward 5'- GCGCCTATGCCAATGAGC-3' Reverse 5'- GCAAGCCTCGCGACCATT-3'	
<i>ChIP apln -3.8 kb</i>	Forward 5'-TAGAGAGGACTGCAGCAGGAT-3' Reverse 5'-CTACCCGTCAAGCAAGGAGA-3'	
<i>ChIP apln -1.6 kb</i>	Forward 5'-GGAGTGGGAAGAGCAGAGATT-3' Reverse 5'-TAGCTGCTGTAGGCCATCACT-3'	
<i>ChIP apln -0.82 kb</i>	Forward 5'-AGGATCCTCCCTACAACGAGA-3' Reverse 5'-AGGCATTCTGCAGGTTCTACC-3'	
<i>ChIP apln TSS</i>	Forward 5'-GCTACAAAATGCAGACCCCCG-3' Reverse 5'-CTCCCAACTACCCGTTGGTC-3'	
<i>ChIP apj -3.9 kb</i>	Forward 5'-TGAAATCACCTCGGGGAGAGA-3' Reverse 5'-GCAGGGTTGTTAGCCAGAGT-3'	
<i>ChIP apj -3.2 kb</i>	Forward 5'-GGCTATTGAAGCTTCATGTTCC-3' Reverse 5'-TCCAGAAAGATCCAGGAGAAC-3'	
<i>ChIP Apj -2.8 kb</i>	Forward 5'-AGTCCCCGGCAGAATTGAGT-3' Reverse 5'-GAGAACACCTGGTGGCTGT-3'	
<i>ChIP Apj -1.0 kb</i>	Forward 5'-TGCTTCTTTCTGCCTCCTCTA-3' Reverse 5'-CAATATCCATGGCCAAGAGGT-3'	
Negative Control	Forward 5'-CACGAGTCCTGGTGACTIONG-3' Reverse 5'-GAGCCATGGAAGAAAAGTTCC-3'	
<i>Arntl</i>	Forward 5'-GGAAAGTAGGTTAGTGGTGCAC-3' Reverse 5'-CAAGTCGGCGCGGGTAAACAGG-3'	

Software and algorithms

GraphPad Prism 9	GraphPad Software Inc.	RRID: SCR_002798
Primer Express™ Software v3.0.1	ThermoFisher Scientific	Cat# 4363991, RRID: N/A
FlowJo 10	Beckton Dickinson & Company	RRID: SCR_008520
AutoQuant	Bitplane	http://www.bitplane.com
Imaris 10.1	Oxford Instruments	RRID: SCR_007370
ImageJ	ImageJ	RRID: SCR_003070
GIANT	Vandel et al. ⁵⁰	
DiscoRhythm v1.2.1	https://mcarlucci.shinyapps.io/ discorhythm/ ; Carlucci ⁹¹	
Phantusus v1.25.4	Kleverov et al. ⁹² ; https://doi.org/ 10.7554/eLife.85722	https://artyomovlab.wustl.edu/ phantusus/
FlowJo V 10.6 software	Tree Star	https://www.flowjo.com/solutions/ flowjo/downloads
FACSDiva V 7.0 software BD	BD	https://www.bdbiosciences.com/ en-us/instruments/researchinstruments/research-software/flow-cytometry-acquisition/facsdiva-software

(Continued on next page)

Continued

REAGENT or RESOURCE	SOURCE	IDENTIFIER
Prism V 8.3.0	GraphPad Software	https://www.graphpad.com/scientific-software/prism/
Others		
Standard diet	Safe	Cat# U8231G10R
ALZET® micro-osmotic pumps	Charles River Laboratories	Cat# 10104846

EXPERIMENTAL MODEL AND STUDY PARTICIPANT DETAILS**Mice and ethics statement**

Male specific pathogen-free C57BL/6JRj young-adult mice (2-month-old, 20–25 g) and elderly mice (22-month-old, 35–45 g) were purchased from Janvier Labs (Le Genest-St-Isle, France). *Nr1d1*^{-/-} mice were obtained from Dr Björn Vennström (Karolinska Institutet, Stockholm, Sweden)¹⁹ and backcrossed for 8 generations with 129S1/SvImJ mice. *Apj*^{-/-} mice⁷⁸ (C57BL/6J background) were from Deltagen (San Carlos, CA). As controls, littermates were used. Mice were fed a standard rodent chow (SAFE A04, SAFE, Augy, France) with water *ad libitum* and housed in a 12-h light/dark cycle. All experiments were performed within the biosafety level 2 facility of the Institut Pasteur de Lille and conform to the relevant regulatory standards. The protocols were validated by the local committee (Comité d'Ethique en Experimentation Animale 75, Nord Pas-de-Calais) for the evaluation of the biological risks and complied with current national and institutional regulations and ethical guidelines (Institut Pasteur de Lille/B59-350009). The animal study was authorized by the “Education, Research and Innovation Ministry” under registration number APAFIS#22304-201910011647335v3.

Bacteria

The clinical *S. pneumoniae* isolate E1586 (serotype 1) were described in.⁸⁹

Cell line

Alveolar macrophage-like Max Planck Institute (MPI) cells were a gift from Dr Gyorgy Fejer (University of Plymouth, UK).⁵⁵ This cell line was tested for mycoplasma contamination.

METHOD DETAILS**Diets**

Unless specified, mice were fed a standard rodent chow (SAFE A04) (SAFE, Augy, France) and water *ad libitum*. This diet contains ~11.8% fiber including ~10% water-insoluble fiber (3.6% cellulose) and 1.8% water-soluble fiber.

Infections and assessment of bacterial loads

Mice were anesthetized by intramuscular injection of ketamine 1000 (50mg/kg⁻¹) (Virbac, Carros, France) and xylazine (10mg/kg⁻¹) (Elanco, Sèvres, France), and intranasally infected with 40 µL of Dulbecco modified essential medium (DMEM) (ThermoFisher, #11995065) containing (or not, for mock (control) animals) 1 × 10⁶ colony forming units (CFU) of *S. pneumoniae* serotype 1 (clinical isolate E1586).^{89,90} Mice were infected at different ZTs. ZT0 is defined as the time when the lights are turned on. For tissue collection, animals were euthanized with an intraperitoneal injection of euthasol (40 mg/kg). Sacrifice was performed 24 or 36 h after infection. The lungs were homogenized in sterile phosphate-buffered saline (PBS) before being diluted and plated on Trypticase soy agar with 5% sheep blood (BioMérieux, Marcy l'Etoile, France) (#43001). The plates were incubated at 37°C with 5% CO₂ for 24 h and viable bacteria were counted. In survival experiments, mice were euthanized when reaching a defined illness score validated for *S. pneumoniae* infection and predicting death of the animal within short time. The score included several morbidity criteria (ruffled fur, breathing, movement) and high body weight loss, according to the legal requirements. Euthanized mice were noted as dead in the survival analyses.

Stimulation of pulmonary mononuclear cells and ELISA

Lungs were obtained from young-adult and elderly mice at ZT0 and ZT12. Briefly, lungs were perfused with PBS, excised and finely minced with a razor blade, followed by enzymatic digestion for 60 min at 37°C with a mix of DNase I (1 µg/mL, Sigma-Aldrich) and collagenase D (400 U/mL, Roche, Basel, Switzerland) 1 µg/mL and incomplete RPMI-1640 medium (ThermoFisher, #11875119). After incubation, tissue-pieces were passed through a 70 µm nylon cell strainer (Corning, Durham, NC) and the single cell suspensions were collected by centrifugation. Pelleted cells were resuspended in 2 mL red blood cell lysis buffer (Life Technologies, Carlsbad, CA) (#00-4333-57) and incubated at room temperature for 5 min. To stop the reaction, RPMI-1640 completed with essential and non-essential amino acid, penicillin, streptomycin, HEPES, sodium pyruvate, L-glutamate (all from Sigma Aldrich), and 10%

heat-inactivated fetal bovine serum (Gibco, ThermoFisher, #A5670701) (complete RPMI) was added. Lung mononuclear cells (2×10^5 /well, 96-well plates) were stimulated for 24 h with R848 (10 µg/mL), CpG ODNs (10 µg/mL) or LPS (1 ng/mL) (all from InvivoGen, San Diego, CA). IL-12p40, and IFN- γ concentrations were measured by ELISA accordingly to protocol's manufacturer (Invitrogen, Waltham, MA) (#88-7120-88 and #88-7314-88, respectively).

Rev-erb agonist/antagonist treatment, depletion of alveolar macrophages, and apelin treatment

The Rev-erb agonist (SR9009) and antagonist (SR8278) were purchased from Tocris Bioscience (Bristol, UK). Apelin ([Pyr1]-Apelin-13) was purchased from Sigma Aldrich (Saint Quentin-Falavier, France). Clodronate liposomes and empty liposomes were obtained from Liposoma Technology (Amsterdam, The Netherlands). Anesthetized mice were treated via the intranasal route with 20 µL of SR9009 (25 mg/kg) or SR8278 (25 mg/kg) at ZT9 and ZT12. Mice were then intranasally infected with *S. pneumoniae* as described above. During the procedure, anesthesia was maintained with isoflurane. To deplete alveolar macrophages, mice were intranasally treated with 50 µL clodronate liposomes. Treatment was performed 24 h before SR8278 inoculation. To maintain a constant blood level of apelin, ALZET micro-osmotic pumps (Charles River Laboratories, Lyon, France) (#10104846) (14-day delivery at 0.11 µL/h rate) were inserted subcutaneously. Briefly, pumps were filled with 100 µL of PBS or apelin (50 µg) and kept overnight at 37°C in PBS. The next day, mice were anesthetized and the pumps were inserted subcutaneously. Mice were treated with 200 µL buprenorphine subcutaneously (0.15 mg/kg) two times at 8 h interval to manage pain. Mice were infected with *S. pneumoniae* seven days after the implantation of the osmotic pumps. For Rev-erb antagonist and apelin co-treatment, elderly mice were implanted with the osmotic pump and seven days later mice were treated with SR8278 as described above.

SR8278 incorporation into nanoparticles

The biodegradable acid-terminated poly(lactic-co-glycolic acid) (PLGA) (50:50 lactic acid:glycolic acid, molecular weight = 5–20 kDa) copolymer (#EXPANSORB 10P019) and acid-terminated poly(lactic acid) (PLA) (18–24 kDa) (#EXPANSORB 10P005) were purchased from Seqens (Aramon, France) and Sigma-Aldrich, respectively. To encapsulate SR8278 in PLGA-based nanoparticles, 60 mg of PLGA and 10 mg of SR8278 were dissolved in 1.5 mL of dichloromethane (Sigma-Aldrich) and emulsified using 4 mL of a 0.5% w/v poly(vinyl alcohol) (88% hydrolyzed, Sigma-Aldrich) aqueous solution by vortexing for 20 s. The emulsion was further sonicated for 90 s (20% power) and 30 s (10% power), using a sonicator probe (Bandelin Sonopuls HD 2070, Berlin, Germany). Dichloromethane was allowed to evaporate overnight under magnetic stirring. Empty nanoparticles were also prepared as controls. SR8278 encapsulation rates were determined by high-performance liquid chromatography (HPLC, Agilent 1100 Series, Les Ulis, France), using a ODS-3 C18 column (4.6 × 250 mm, 5 mm) (Phenomenex Le Pecq, France), a mobile phase consisting of Milli-Q water:acetonitrile (gradient grade for HPLC, Sigma-Aldrich) 10:90, a flow rate of 1 mL/min, and a detection wavelength of 310 nm. The encapsulation rate was 90.8%. The stock solution contains 15 mg nanoparticles/mL (2.5mg SR8278/mL). Fluorescent nanoparticles were prepared by adding 0.2 mg of PLA grafted with rhodamine B (Sigma-Aldrich) into dichloromethane before emulsification. To perform nanoparticles characterization, dynamic light scattering, nanoparticle tracking analysis, transmission electron microscopy and fluorescent confocal microscopy analyses were performed as previously described.⁹³

RNA extraction, RNA sequencing analysis and statistical analysis

Lungs from young-adult mice and elderly mice were harvested at ZT0, ZT4, ZT8, ZT12, ZT16 and ZT20 ($n = 4$ –5/group), incubated in RNA later for 10 min at room temperature and frozen in liquid nitrogen. Total RNA was extracted with Trizol and purified on NucleoSpin RNA column (Macherey Nagel, Düren, Germany) (#740955.50). The quality of RNA was evaluated with a Bioanalyzer (Agilent Technologies) and the Agilent RNA 6000 nano kit (#5067-1511). Only RNAs with RNA Integrity Number (RIN) over 7 were used. 200ng of RNA were used for library construction followed by 100 bp paired-end sequencing performed by DNBSEQ technology and DNA nanoballs. The primary analysis of raw sequencing datasets was performed using the nf-core/rnaseq v3.6 pipeline (<https://doi.org/10.5281/zenodo.7998767>). Raw FastQ files were quality and adapter trimmed with Trim Galore v0.6.7. (https://www.bioinformatics.babraham.ac.uk/projects/trim_galore/). Ribosomal RNA reads were filtered out with SortMeRNA v 4.3.4.⁹⁴ Cleaned reads were aligned with STAR v2.6.1d⁹⁵ against the GRCh38 genome from the Ensembl 108 database and expression for annotated genes was quantified using Salmon v1.5.2⁹⁶ in mapping-based mode. Analysis of circadian genes was performed using R (version 4.1.2). Gene counts were normalized using DESeq2 R package.^{94,97} Detection of genes with a circadian rhythm was done with RAIN.⁴³ Raw p -values from RAIN were adjusted for multiple testing using the Benjamini-Hochberg procedure to control the FDR. Over-representation enrichment analysis was performed with clusterProfiler R package⁹⁸ using Over-Representation Analysis.

Microarray analysis and statistical analysis

Lungs from young-adult and elderly mice were harvested at ZT0 and ZT12 ($n = 4$ /group) and RNAs were extracted as described above. 300ng of RNA was amplified with GeneChip WT PLUS Reagent Kit (Thermo Fisher Scientific) (#902281), labeled with GeneChip WT Terminal (#902281). The resulting single-stranded cDNAs were hybridized on the GeneChip Mouse Gene 2.0 ST Array (Applied Biosystems, Waltham, MA) (#902119) according to the manufacturer's protocol. The microarray data were analyzed using GIANT (version v0.0.2) tools suite⁵⁰ on a local instance of Galaxy.⁹⁹ Data were normalized by the Robust Multi-Average method. Transcripts associated with annotated genes were selected for analysis. Differentially expressed genes were identified by using limma¹⁰⁰ and Raw p values were adjusted for multiple testing using the Benjamini-Hochberg procedure to control the False Discovery Rate

(FDR). To identify genes whose circadian regulation is affected by aging, differential analysis with interaction between age and time-of-day variables was performed. To visualize data, PCA analysis and heatmap were performed with Phantasus⁹² (version v1.25.5) and volcano plot was generated with GraphPad Prism (Boston, MA) (version v10.2.3).

Assessment of gene expression by quantitative RT-PCR

RNAs were reverse-transcribed with the High-Capacity cDNA Archive Kit (Thermo Fisher Scientific) (#4374966). The resulting cDNA was amplified using SYBR Green-based real-time PCR (#4334973) and the QuantStudio 12K Flex Real-Time PCR Systems (Applied Biosystems). Specific primers were designed using Primer Express software (Applied Biosystems) and ordered to Eurofins Scientifics (Ebersberg, Germany). Relative quantification was performed using the gene encoding glyceraldehyde 3-phosphate dehydrogenase (Gapdh). Relative mRNA levels ($2^{-\Delta\Delta Ct}$) were determined by comparing (a) the PCR cycle thresholds (Ct) for the gene of interest and the house keeping gene Gapdh (ΔCt) and (b) ΔCt values for treated and control groups ($\Delta\Delta Ct$). Data was expressed as a fold-increase over the mean gene expression level in young mice (ZT0). Cosinor analysis was performed using GraphPad prism 10.

Chromatin immunoprecipitation assay

Chromatin immunoprecipitation (ChIP) experiments were performed on young lungs harvested at ZT10.⁹³ Briefly, lungs were extracted in a hypotonic buffer containing HEPES-KOH 50 mM pH7.5, Triton X-100 0.25%, Glycerol 10%, EGTA 0.5 mM, EDTA 1 mM, NaCl 140 mM, NP-40 0.5%, protease inhibitor cocktail (Roche Diagnostics, Basel, Switzerland). After 10 min incubation, nuclei were washed with a buffer containing Tris-HCl 10 mM, pH8.0, EGTA 0.5 mM, EDTA 1 mM, NaCl 200 mM and protease inhibitor cocktail. DNA and protein were then cross-linked in paraformaldehyde 1% for 10 min at room temperature. PFA was quenched using glycine 200 mM for 10 min at room temperature. Nuclei were lysed in Tris-HCl 50 mM pH8.0, EDTA 10 mM, SDS 1% and protease inhibitor cocktail and DNA fragment of 150–200 bp were generated using a Bioruptor (20 cycles 30 secondes On/30 secondes Off). Immunoprecipitation was performed using the anti-Rev-erb- α antibody (1/50, #13418, Cell Signaling Technology, Danvers, MA) or the anti-H3K27me3 antibody (1/100, #ab6002, Abcam, Cambridge, MA). Purified DNA was subjected to 40 cycles of PCR amplification. Specific primers were ordered to Eurofins Scientifics. Crossing threshold (Ct) values were determined for each promoter and normalized to the Ct of input using the following equation: relative values = $2^{-(Ct_{IP} - Ct_{input})}$. Data were expressed as a fold induction compared with the negative region using $2^{-\Delta\Delta Ct}$ with $2^{-[(Ct_{IP \text{ region of interest}} - Ct_{input}) - (Ct_{IP \text{ negative region}} - Ct_{input})]}$.

Flow cytometry

Lung MNCs were prepared as described above. Lungs were excised into 1 mm³ fragments, then enzymatically digested for 30 min in RPMI supplemented with 1 mg/mL collagenase type VIII (Sigma-Aldrichn Saint-Louis, MI, USA) at 37°C. RMPI was added and digested lung tissues were centrifuged at 400g for 10 min. Cells pelleted were resuspended in a 20% Percoll solution (Percoll GE Healthcare C, Chicago, IL, USA) and centrifuged at 500g for 15 min at 20°. Cell pellets were resuspended in red blood cell lysis buffer (Red Blood Cell Lysing Buffer Hybri-Max, Sigma-Aldrich) for 5 min. After centrifugation at 400g for 10 min, cells were incubated for 20 min at 4°C in 2.4G2 hybridoma supernatant (FC gamma blocking antibody) diluted in PBS containing 5% FBS, 0.01% NaN3 (FACS buffer). Cells were washed and resuspended in FACS buffer before being pelleted and stained (30 min, at 4°C) with the fluorochrome-conjugated antibodies against mouse CD45 (Pacific Blue-, Brilliant Violet 510- or AF700-coupled), CD19 (BV-510-coupled), anti-TCR β (PECy7-coupled), anti-CD4 (APCCy7-coupled), anti-CD8 (FITC-coupled), anti-TCR $\gamma\delta$ (PerCpCy5.5-coupled), anti-TCR β (PECy7-coupled), anti-NK1.1 (PE-coupled), anti-CD11b (PerCpCy5.5-coupled), anti-Ly6G (APCCy7-coupled (APCCy7-coupled)), anti-CD64 (APC-coupled), anti CD11c (PECy7-coupled), anti-MHCII (AF700-coupled), anti-CD103 (FITC-coupled) (1/100), anti-CD3 (APCCy7-coupled), anti-F480 (FITC-coupled), anti-Ly6C (AF700-coupled) (all from BioLegend, San Diego, CA), and anti-Siglec F (PE-coupled) (BD Biosciences, Franklin Lakes, NJ) (dilution 1/500-1/1000). Cells were washed twice by centrifugation and resuspended in FACS buffer prior to being analyzed on a BD LSR II Fortessa cytometer (BD Biosciences). Data was analyzed using FlowJo Software (FlowJo LLC, Ashland, OR). Dead cells were excluded on the basis of scatter (SSC) and DAPI exclusion. To assess intracellular cytokine production, lung MNCs were incubated in RPMI 1640 5% FCS containing Golgi Plug/Golgi Stop (BD Biosciences) for 2 h at 37°C and then stained with appropriate dilutions of antibodies (30 min, 4°C) in PBS 2% FCS. Cells were stained with PE-conjugated mAb against IL-17A (BioLegend) or PE-conjugated control rat IgG1 mAb. Cells were washed and fixed by using intracellular fixation buffer (eBioscience, CliniSciences, Montrouge, France). Fixed cells were then permeabilized in permeabilization buffer (eBioscience) according to the manufacturer's instructions and then taken to FACS.

To analyze the expression of endocytic receptors on MPI cells, cells were labeled with the following antibodies: anti-CD45 (BV605-coupled), anti-CD11b (AF700-coupled), F480 (FITC-coupled), CD206 (PECy5-coupled), CD204 (APC-coupled) and CD36 (APCFire750-coupled) (all from BioLegend, San Diego, CA). To assess internalization of nanoparticles *in vivo*, AMs (3–5 × 10⁶ cells) were labeled with the following antibodies: FITC-coupled anti-CD11c (1/200), BV421-coupled anti-Siglec F (1/200), allophycocyanin (APC)-coupled anti-F4/80 (1/200) (all from BD Biosciences). Fixable viability dye aqua (Thermo-Fisher) was used to gate viable cells.

In vitro phagocytosis, ROS production and killing assay (MPI cells)

MPI cells were grown in complete RPMI and GM-CSF (PeproTech, Cranbury, NJ) (#315-03) (30 ng/mL) as described.¹⁰¹ MPI cells (5 × 10⁵/well in 24-well plate) were synchronized with 50% horse serum (Fisher Scientific, #10368902) for 2 h, washed with PBS at 37°C and then maintained in complete RPMI for 10 h before stimulation. To measure phagocytosis and killing activity, SR8278 (2 μ M),

apelin (5 µg/mL), SR8278 (2 µM) plus apelin (5 µg/mL), or vehicle was added for 1 h. Cells were then washed three times with PBS at 37°C to remove antibiotics. Opsonized *S. pneumoniae* was added to the cells at multiplicity of infection of 10 (MOI 10 and incubated at 4°C for 1 h to induce adherence, and at 37°C for 1.5 h for internalization). Non-internalized bacteria were removed by washing with PBS at 37°C with penicillin and streptomycin (30 U/mL) and cells were then incubated for 30 min in RPMI with 10% FBS and penicillin and streptomycin (30 U/mL). For phagocytosis (2 h post *S. pneumoniae*), cells were washed to remove remaining antibiotics, lysed with cold sterile water, and plated onto TSA 5% sheep blood agar. For killing (5 h post *S. pneumoniae*), cells were incubated for 2.5 h with penicillin, streptomycin, and vancomycin (0.75 µg/mL), and plated onto Trypticase Soy Agar 5% sheep blood agar. Phagocytosis was calculated as an increase percentage of phagocytosis in the SR8278 group over the vehicle group (% of phagocytosis = CFU final x 100/CFU final average of vehicle group). Macrophage killing activity was calculated as % of killed bacteria = [viable bacteria at killing time point (CFU 3 h post infection – CFU 5 h post infection)*100/viable bacteria at killing time point average of vehicle group]. Confocal microscopy was also performed to quantify the numbers of engulfed bacteria (4 h post *S. pneumoniae*). For this, 5 x 10⁵/well MPI cells were seeded in 8-well plate, synchronized, SR8278, SR9009 or apelin treated (1 h) and incubated (4 h) with eGFP-expressing *S. pneumoniae* (MOI 10), a gift from Dr Jose A. Chabalgoity (Montevideo, Uruguay). To quantify ROS generation by macrophages, CellROX Oxidative Stress Reagents (Life technologies, #C10422) were added 30 min before fixation. Cells were fixed with PFA 4%, washed with PBS-T (0.1% Tween 20), and blocked with 1% BSA for 1 h, and incubated with phalloidin Alexa Fluor 546 (Life Technologies, Carlsbad, CA) (#A22283, 1:500) for 30 min at room temperature, washed with PBS, and then incubated with Hoechst (1/1000) for 30 min. Cells were washed and mounted using fluorescence mounting medium (Dako Omnis, Agilent). Images were acquired using Zeiss LSM 880 AiryScan microscopy (Carl Zeiss, Rueil-Malmaison, France) and processing using Imaris 10.1 (Oxford Instruments, Les Ulis, France) and ImageJ software (National Institutes of Health, Wisconsin). Synchronized MPI cells were also exposed to pHrodo Red Zymozan A bioparticles conjugates (Invitrogen, #P35364) (0.2 mg/ml). The later allow measurement of the internalization rate of the bioparticles (which are pH sensitive), thus assessing the fusion of endocytic vesicles to lysosomes. The bioparticles were prepared in Opti-MEM culture medium (Invitrogen # 31985-062) containing Hoechst 33342 20 µM (Thermo Scientific #62249), allowing labeling of cell nuclei for imaging acquisition. Phagocytosis was measured after 2 h using an automated fluorescent confocal microscope (In Cell analyzer 6000, GE Healthcare, Chicago, IL) equipped with a 20X (NA 0.70) air lens or 60X (NA 1.2) water lens (Nikon, Tokyo, Japan).

Collection of alveolar macrophages and phagocytosis assay

Alveolar macrophages were collected from bronchoalveolar lavages of wild type, *Nr1d1*^{-/-} and *Apj*^{-/-} mice at ZT0. To this end, 1000 µL of ice-cold PBS was instillated via the exposed trachea into the lungs, followed by aspiration after 30 s, using a 24G IV cannula (BD Insite-w, Franklin Lakes, NJ) (#381312). Alveolar macrophages were collected by centrifugation at 10,000 x g for 2 min, discarded in 24-well plate and then exposed to *S. pneumoniae* (MOI 10) for 2 h. *In vitro* phagocytosis assay was performed as described above (lysis).

Generation of bone marrow-derived macrophages (BMDMs) and phagocytosis assay

Murine bone-marrow progenitors were obtained by sampling tibias and femur bones from *Nr1d1*^{+/+} and *Nr1d1*^{-/-} mice. BMDMs were obtained by seeding bone marrow cells in 75 cm² flasks in RPMI 1640 Glutamax medium (Gibco) supplemented with antibiotics, 10% heat-inactivated FBS and macrophage colony stimulating factor (M-CSF, 10 ng/mL) (Preprotech, #AF-315-03-B). After 7 days incubation, BMDMs were transferred (20. 000 cells/well) into 96-well plate. For phagocytosis assay, BMDMs were shock serum-synchronized and, 23 h later, were exposed to eGFP-expressing *S. pneumoniae*. Confocal microscopy was performed to quantify the numbers of cells that had engulfed bacteria (4 h). ROS production was measured as described above.

Analysis of circadian phagocytosis (BMDMs)

Nr1d1^{+/+} and *Nr1d1*^{-/-} BMDMs were transferred (20. 000 cells/well) into 384-well plate (Dutscher, #781091). Synchronized BMDMs were exposed to pHrodo Red Zymozan A bioparticles (0.2 mg/ml) conjugates for 30 min. Phagocytosis was measured using an automated fluorescent confocal microscope (In Cell analyzer 6000) equipped with a 20X (NA 0.70) air lens or 60X (NA 1.2) water lens (Nikon). The confocal microscope was equipped with 405, 488, 561 and 642 nm excitation lasers. The emitted fluorescence was captured using a camera associated with a set of filters covering a detection wavelength ranging from 450 to 690 nm. Hoechst 33342-stained nuclei were detected using the 405 nm laser with a 450/50-nm emission filter. pHrodo Red signal was recorded using 561 nm laser with 600/40-nm emission filters. Images from the automated confocal microscope were analyzed using multi-parameter scripts developed using Columbus system (version 2.3.1, PerkinElmer). We applied segmentation algorithms to input images, allowing us to distinguish nuclei and intracellular bioparticles and to determine the percentage of infected cells and the intracellular particle load per cell. Briefly, the host cell segmentation was performed using two different Hoechst signal intensities -a strong intensity corresponding to the nucleus and a weak intensity in cytoplasm -with the algorithm “Find Nuclei” and “Find Cytoplasm”. Red signal intensities in a cell were used for the intracellular bioparticles segmentation with the algorithm “Find Spots”. Subsequently, the population of red positive cells was determined, and the increase of intracellular red bioparticles was calculated.

Western blotting

Lung extracts were lysed in RIPA buffer (50 mM Tris-HCl pH8.0, 150 mM NaCl, 1% NP-40, 0.5% sodium deoxycholate and 0.1% SDS supplemented with protease inhibitors (Roche Diagnostics, Meylan, France) (#11836170001), heated at 95°C for 20 min, and centrifuged at 10,000g for 10 min. Proteins in supernatants were quantified using the Pierce BCA protein assay kit (Thermo Fisher Scientific) (#23225). An equal amount of protein was mixed with Laemmli loading buffer (EcoTech Biotechnology, Istanbul, Turkey). Proteins were then separated using 12% SDS-PAGE and then transferred from the gel to a nitrocellulose membrane. The polyclonal rabbit antibody directed against APJ was from Abcam (1:1000, #ab308018). The detection was made by using the appropriate horse-radish peroxidase-conjugated secondary antibody (1/2500, #ab6721, Abcam). Antibodies were detected using chemiluminescence (Pierce), and the signals were quantified by applying the “gel quantification” procedure in ImageJ software (version1.1.0) (National Institutes of Health). To normalize, an antibody directed against β-actin was used (#A5441, 1/1000, Sigma-Aldrich).

QUANTIFICATION AND STATISTICAL ANALYSIS

Excepted for the transcriptomic analyses, all statistical analyses were performed using GraphPad Prism 8 software. A two tailed Mann-Whitney *U* test was used to compare two groups. Comparisons of more than two groups with each other were analyzed with the one-way ANOVA Kruskal-Wallis test (non-parametric), followed by a Dunn's or a Dunnett's post-hoc test or using the two-way ANOVA followed by a Tukey's multiple comparisons post-hoc test, a Sidak post-hoc test or a Newman-Keuls post-hoc test. The survival of infected mice was analyzed using the log rank test. Statistical analysis of rhythmicity was assessed using JTK_Cycle (DiscoRhythm,⁹¹ <https://mcarlucci.shinyapps.io/discoRhythm/>). The symbol “*n*” represent the number of mice or biological replicates in the experiments. Except for the determination of the bacterial load where the bar represents the median and for the transcriptomic analyses, *in vivo* and *ex vivo* data are expressed as mean ± Standard Error of the Mean deviation (SEM). *In vitro* data are expressed as the mean ± Standard Deviation (SD).